Transition strengths and degree of deformation in ^{79}Sr

R. A. Kaye,[1,2] Y. K. Ryu,[1] S. R. Arora,[1,*] S. L. Tabor,[2] J. Döring,[3,†] Y. Sun,[4,5] T. D. Baldwin,[2,‡] D. B. Campbell,[2,§] C. Chandler,[2,‖] M. W. Cooper,[2,¶] S. M. Gerbick,[2,6,**] O. Grubor-Urosevic,[6] C. R. Hoffman,[2] J. Pavan,[2,††] L. A. Riley,[7,‡‡] and M. Wiedeking[2,††]

[1]*Department of Physics and Astronomy, Ohio Wesleyan University, Delaware, Ohio 43015, USA*

[2]*Department of Physics, Florida State University, Tallahassee, Florida 32306, USA*

[3]*Gesellschaft für Schwerionenforschung (GSI), Planckstr. 1, D-64291 Darmstadt, Germany*

[4]*Department of Physics and Joint Institute of Nuclear Astrophysics, University of Notre Dame, Notre Dame, Indiana 46556, USA*

[5]*Department of Physics, Xuzhou Normal University, Xuzhou, Jiangsu 221009, People's Republic of China*

[6]*Department of Chemistry and Physics, Purdue University Calumet, Hammond, Indiana 46323, USA*

[7]*Department of Physics and Astronomy, Earlham College, Richmond, Indiana 47374, USA*

(Received 27 November 2006; published 22 March 2007)

High-spin states in ^{79}Sr were studied using the ^{54}Fe(^{28}Si,2pn) reaction at 90 MeV, with a thick 14-mg/cm^2 ^{54}Fe target used to stop all recoils. Prompt γ-γ coincidences were detected using the Florida State University Compton-suppressed Ge array consisting of three Clover detectors and seven single-crystal detectors. The most recent ^{79}Sr level scheme has been confirmed in three separate band structures up to a spin as high as the $(\frac{37}{2}^+)$ yrast state based on γ-ray coincidence relations, intensity and effective lifetime measurements, and directional correlation of oriented nuclei ratios. Lifetimes of 33 excited states were measured using the Doppler-shift attenuation method, with the experimental line shapes obtained at two separate observation angles and by gating from above the transitions of interest whenever possible. Transition quadrupole moments Q_t inferred from the lifetimes indicate a high degree of collectivity and deformation over a rather wide range of spins in all three observed bands, with evidence for modest reductions in the values with increasing spin. The changes in Q_t are attributed to the onset of quasiproton alignment and are supported qualitatively by the predictions of the projected shell model and cranked Woods-Saxon calculations in conjunction with the cranked shell model. Lifetimes measured in a band based on the $[431]\frac{1}{2}^+$ intrinsic Nilsson configuration suggest a large quadrupole deformation ($\beta_2 \approx 0.41$) associated with this band, providing another example of the strong deformation-driving properties of the $d_{5/2}$ intruder orbital in the mass 80 region.

DOI: 10.1103/PhysRevC.75.034311 PACS number(s): 21.10.Tg, 23.20.Lv, 27.50.+e

I. INTRODUCTION

The light, proton-rich strontium isotopes have been known [1] to exhibit large prolate deformation at low excitation energy for some time. With both proton and neutron numbers near the middle of the *f-p-g* shell, correlating to a relatively large number of valence particles, the ground states of these nuclei are primed to possess some of the strongest quadrupole deformations β_2 in the mass 80 region [2]. These large deformations could be expected to persist at high spin due to the significant gap in the single-particle energy spectrum at particle number 38 for a prolate deformation of $\beta_2 \approx 0.4$ [3], resulting in a large energy cost associated with promoting quasiprotons above the gap.

The neutron Fermi levels for these nuclei lie in the vicinity of the $[422]\frac{5}{2}^+$ and $[301]\frac{3}{2}^-$ Nilsson orbitals, as well as the $[431]\frac{1}{2}^+$ orbital which intrudes from the $d_{5/2}$ subshell. The intrinsic structure of light odd-mass Sr isotopes is therefore expected to be influenced by quasineutron occupation of these three orbitals. In ^{81}Sr, band structures suggested to be based on these intrinsic configurations have been found and well studied [4–7]. Lifetime measurements at low spin [4] followed by more measurements at high spin [5,6] showed that although the yrast positive- and negative-parity bands (based on the $[422]\frac{5}{2}^+$ and $[301]\frac{3}{2}^-$ configurations) exhibited moderate collectivity (with transition quadrupole moments $|Q_t| \approx 2.0\ e$b), the band based on the $[431]\frac{1}{2}^+$ configuration had a large average Q_t value of $\pm 3.5\ e$b, corresponding to an axial deformation of $\beta_2 \approx 0.4$ [5,6]. The much larger collectivity associated with the $[431]\frac{1}{2}^+$ band was attributed [6] to core polarization caused by quasineutron occupation of the $d_{5/2}$ intruder orbital.

The next lightest odd Sr isotope, ^{79}Sr, is expected to behave similarly to ^{81}Sr. Indeed, rotational structures grouped

*Present address: Department of Applied Physics and Applied Mathematics, Columbia University, New York, New York 10027, USA.

†Present address: Bundesamt für Strahlenschutz, D-10318 Berlin, Germany.

‡Present address: Department of Physics, University of Surrey, Guildford, Surrey, GU2 7XH, United Kingdom.

§Present address: Lawrence Livermore National Laboratory, Livermore, California 94551, USA.

‖Present address: School of Chemistry and Physics, Keele University, Keele, Staffordshire, ST5 5BG, United Kingdom.

¶Present address: Pacific Northwest National Laboratory, Richland, Washington 99352, USA.

**Present address: Physics Division, Argonne National Laboratory, Argonne, Illinois 60439, USA.

††Present address: Nuclear Science Division, Lawrence Berkeley National Laboratory, Berkeley, California 94720, USA.

‡‡Present address: Department of Physics and Astronomy, Ursinus College, Collegeville, Pennsylvania 19426, USA.

into bands based on the $[422]\frac{5}{2}^{+}$ and $[301]\frac{3}{2}^{-}$ configurations have been assigned and studied by a variety of previous experimental investigations [1,8–12]. A band suggested to be based on the $[431]\frac{1}{2}^{+}$ configuration was also found [11] and later verified by the most recent study of ^{79}Sr [12], which also extended the level scheme to the highest known spins in each band, reaching $I^{\pi} = \frac{45}{2}^{+}$, $\frac{45}{2}^{-}$, and $\frac{41}{2}^{+}$ in the $[422]\frac{5}{2}^{+}$, $[301]\frac{3}{2}^{-}$, and $[431]\frac{1}{2}^{+}$ bands, respectively. Nevertheless, lifetime information in these bands remains limited, particularly for the higher spin states. The large quadrupole moments in the low-spin states of the yrast negative-parity band deduced from angular distributions [1] were later verified by lifetime measurements using the recoil-distance and Doppler-shift attenuation methods [8,10]. Further lifetime measurements of states in the yrast positive-parity band using direct timing [9], and the recoil-distance and Doppler-shift attenuation methods [8], also revealed a high degree of collectivity ($|Q_{t,\mathrm{ave}}| = 2.9\,e$b) based on the $E2$ transition rates. However, mean lifetime measurements are not available for spins at or above the band-crossing regions [8,9,12] for each of these bands, where the observed quasiproton alignment was rather sharp in the yrast positive-parity band, but only very gradual in the yrast negative-parity band based on the behavior of the moments of inertia [9]. The differences in the alignments were explained [9] in terms of the different favored structures in the alignment regions of each band. The yrast positive-parity band was predicted to have a triaxial shape with reduced deformation ($\beta_2 \approx 0.32$) in the band-crossing region, evolving from a more deformed ($\beta_2 \approx 0.35$) prolate shape below the crossing. In the yrast negative-parity band, both the deformation ($\beta_2 \approx 0.37$) and the prolate shape were predicted to persist as the nucleus transitions through the band-crossing region. Since transition quadrupole moments are sensitive to structure changes, any difference in their behavior near the region where the quasiproton alignment occurs in each band would provide a test of these predictions. Moreover, lifetimes have not been measured for any states in the $[431]\frac{1}{2}^{+}$ band. Establishing the degree of collectivity and deformation in this band would be a particularly useful test of the available theoretical models, considering that its deformation has long been predicted [3,6] to be the largest among the other bands based on this configuration in the $N = 39$–45 Sr isotopes, a result that has awaited experimental verification. It would also constitute only the second measurement of lifetimes in a band considered to be based on the $[431]\frac{1}{2}^{+}$ intrinsic configuration in this mass region.

The present work was undertaken to measure lifetimes to as high a spin as possible in all three known rotational bands in ^{79}Sr using the Doppler-shift attenuation method (DSAM). As a result of this work, the measured lifetimes have been used to map the evolution of collectivity with increasing spin in both the yrast positive- and negative-parity bands beyond the band-crossing regions, as well as to establish the degree of collectivity and deformation for the first time in the $[431]\frac{1}{2}^{+}$ band. Comparisons to the results obtained for the neighboring $Z = 38$ isotopes and $N = 41$ isotones were performed where data are available, and thus the underlying structure features of ^{79}Sr were compared to the existing systematics available from studies of other light proton-rich nuclei in this mass region. The results of this work were also used as an additional test case for the predictions of the projected shell model [13] and cranked Woods-Saxon [3] calculations, including a determination of the deformed shapes that are consistent with the lifetime measurements.

II. EXPERIMENTAL AND ANALYSIS TECHNIQUE

High-spin states in ^{79}Sr were produced following the ^{54}Fe(^{28}Si,$2pn$) fusion-evaporation reaction at 90 MeV using the Tandem-Superconducting LINAC accelerator at Florida State University (FSU). To optimize the experiment for the detection of Doppler-shifted γ-ray line shapes and hence the measurement of lifetimes using the DSAM, a thick 14-mg/cm^2 ^{54}Fe target was used to stop all recoiling nuclei. Prompt γ-ray coincidences, recorded within a time window of about 100 ns, were detected using the FSU array of Compton-suppressed Ge detectors, consisting of three Clover detectors placed at 90° relative to the beam direction, and single-crystal detectors placed at 35° (2 detectors), 90° (1), and 145° (4). Approximately 9.4×10^8 total coincidence pairs were collected and sorted into a variety of 3000×3000 channel square γ-γ coincidence matrices with a dispersion of 0.9 keV/channel. Both the sorting and analysis of the γ-ray spectra were performed using program GNUSCOPE, a γ-spectrum analysis software package developed at FSU [14].

γ-ray transition energies and intensities were measured from background-subtracted gated spectra projected from a square matrix consisting of coincidences between only the 90° detectors and all other detectors. To minimize the measurement uncertainty due to Doppler-shifted line shapes, the intensities were first determined at 90° and then corrected for angular distribution effects using the a_2 and a_4 angular distribution coefficients measured previously [9]. In some cases, a_2 and a_4 were deduced from transition mixing ratios measured previously [1,8]. These coefficients were then used to deduce A_0, the angle-independent first-order term in the series of Legendre polynomials that describe the experimental intensities as a function of observation angle. When the a_2 and a_4 coefficients were not available for a particular transition, an average value of the measured ones was used, based on the appropriate multipolarity of the transition ($\Delta I = 1$ or $\Delta I = 2$). As a test of the method, the γ-ray intensities measured previously [8,9] in the yrast positive- and negative-parity bands were remeasured, and the results were in generally good agreement with the previous results, except in the case where systematically larger intensities were measured using an inverse reaction [9]. Even in this case, though, the measured branching ratios remained in good agreement with the previous results.

Spin changes were measured based on directional correlation of oriented nuclei (DCO) ratios, defined according to

$$R_{\mathrm{DCO}} = \frac{I_\gamma(\text{at } 35^\circ, 145^\circ;\ \text{gated by } \gamma_G \text{ at } 90^\circ)}{I_\gamma(\text{at } 90^\circ;\ \text{gated by } \gamma_G \text{ at } 35^\circ, 145^\circ)}. \quad (1)$$

To increase the statistics of the DCO ratio measurement, the analysis was performed using a matrix constructed to exploit the angular symmetry of the FSU Ge array, in which both

35° and 145° detector events were sorted against only the 90° detector events. Based on the geometry of the array, if the gate γ_G represents one or more stretched electric quadrupole ($E2$) transitions, then the DCO ratios for stretched $E2$ transitions are expected to be approximately unity, whereas $\Delta I = 1$ transitions yield ratios of about 0.5 if the mixing ratio is small [5]. All obtainable DCO ratios, along with level energies, spins, and relative intensities are given in Table I. These measurements, along with the γ-ray coincidence relationships and measured effective lifetimes (see below), were used to confirm the existing level scheme of ^{79}Sr [12] (see Sec. III A). A partial level scheme of ^{79}Sr, as deduced from the present work, is shown in Fig. 1.

Doppler-shifted line shapes measured at 35° (145°) were obtained from background-subtracted spectra projected from matrices consisting of coincidence events between 35° (145°) detectors and 90° detectors. This choice increased the likelihood of creating cleaner 35° or 145° coincidence spectra when gating on higher-lying transitions since γ-ray Doppler shifting is minimized at 90°, and thus narrower gates could be set than if coincidences between the 35° or 145° and all other detectors were used. It was then possible to more often pursue a line-shape analysis by gating from above the transition of interest. About 5.7×10^7 (1.4×10^8) coincidence pairs were collected in the 35° (145°) versus 90° detectors matrix.

Mean lifetimes of excited states in the bands shown in Fig. 1 were then measured by applying the DSAM to the experimental line shapes of coincident γ rays detected at 35° and 145°. The DSAM applied to this experiment involved a comparison of the decay time of the recoiling nuclei with their slowing-down time in a thick target. This comparison was carried out using the simulation code FITS [5], which integrates over the thickness of the target and determines a Gaussian distribution of recoil velocities (with a width that is 10% of the kinematic mean) at the time of decay, thus accounting for the evaporation of charged particles in the reaction. It corrects for direct feeding from up to four known higher-lying states and side feeding from one unknown state, as well as for finite detector solid angle and resolution, and the energy dependence of the reaction cross sections as the beam slows through the target. The nuclear and electronic stopping powers were obtained from the program SRIM2000 [15,16].

By varying the lifetime of the parent state of interest, a set of theoretical line shapes was produced and compared with the measured Doppler-shifted spectrum at 35° and 145° to find the best fit. The lifetime that generated a curve that had the lowest

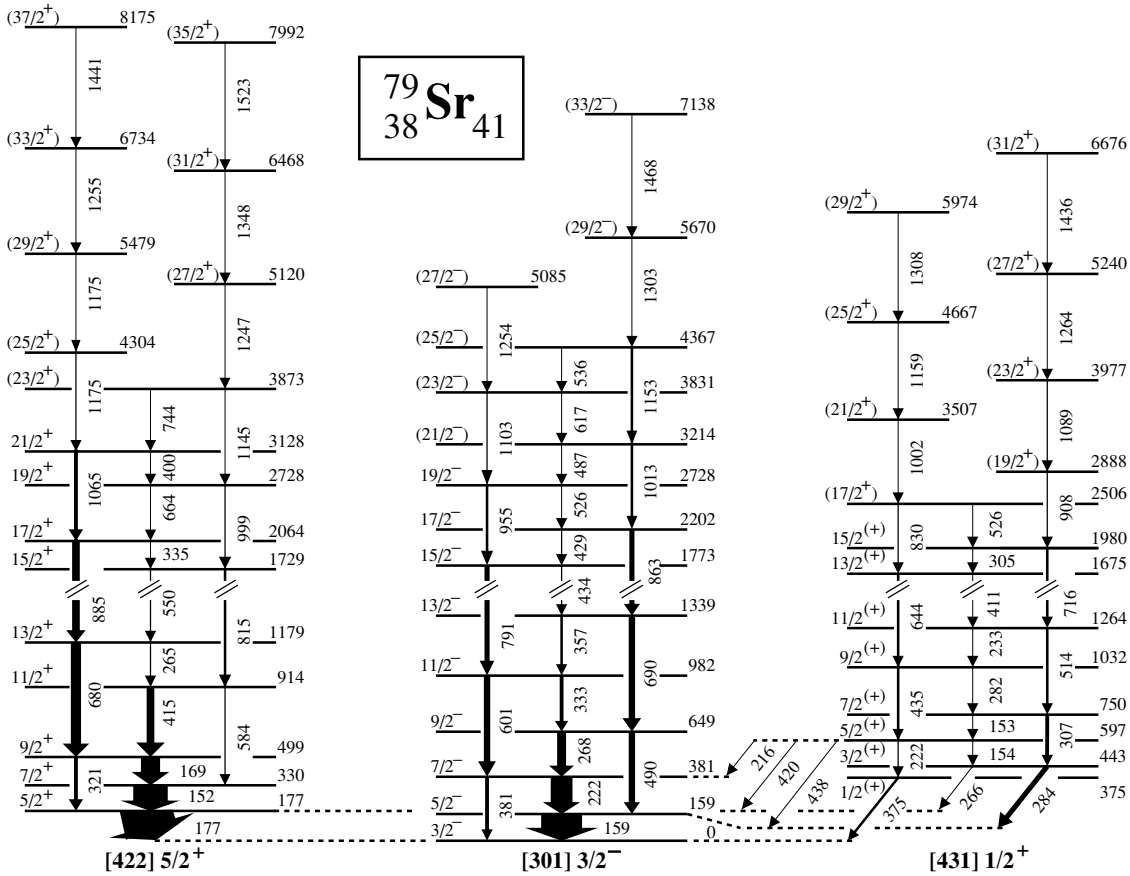

FIG. 1. A partial level scheme of ^{79}Sr, as deduced from the present work. Each band structure has been labeled according to its Nilsson assignment [12]. The vertical energy scale is compressed by a factor of 2 above an excitation energy of 1500 keV, and the widths of the arrows are approximately proportional to the intensity of the corresponding γ-ray transitions. The vertical displacements of the 284- and 438-keV transitions have been exaggerated for clarity.

TABLE I. Excitation energies, initial and final spin states, γ-ray transition energies, relative intensities, and DCO ratios in ^{79}Sr.

E_x (keV)	I_i^π	I_f^π	E_γ (keV)	A_0	R_{DCO}[a]
		$[422]\frac{5}{2}^+$ Band			
177.2(1)	$\frac{5}{2}^+$	$\frac{3}{2}^-$	177.2(1)	118(4)[b]	0.59(4)
329.6(1)	$\frac{7}{2}^+$	$\frac{5}{2}^+$	152.4(1)	85(4)	0.43(4)
498.6(2)	$\frac{9}{2}^+$	$\frac{7}{2}^+$	169.0(1)	48(2)	0.41(3)
		$\frac{5}{2}^+$	321.4(2)	13.0(8)	0.94(11)
913.7(3)	$\frac{11}{2}^+$	$\frac{9}{2}^+$	415.1(1)	20.5(6)	0.26(2)
		$\frac{7}{2}^+$	584.1(3)	8.4(8)	
1178.6(4)	$\frac{13}{2}^+$	$\frac{11}{2}^+$	264.9(2)	7.1(5)	0.44(6)
		$\frac{9}{2}^+$	680.0(3)	26(1)	1.01(10)
1728.9(4)	$\frac{15}{2}^+$	$\frac{13}{2}^+$	550.3(2)	6.2(4)	0.24(8)
		$\frac{11}{2}^+$	815.2(3)	11.1(9)	
2063.7(6)	$\frac{17}{2}^+$	$\frac{15}{2}^+$	334.8(5)	3.4(3)	0.38(11)
		$\frac{13}{2}^+$	885.1(3)	21(2)	1.14(22)
2728.0(7)	$\frac{19}{2}^+$	$\frac{17}{2}^+$	664.3(4)	3.3(7)	0.34(7)
		$\frac{15}{2}^+$	999.1(5)	6.0(7)	
3128.5(8)	$\frac{21}{2}^+$	$\frac{19}{2}^+$	400.5(4)	1.9(3)	
		$\frac{17}{2}^+$	1064.8(5)	13(1)	1.13(17)
3873(1)	$(\frac{23}{2}^+)$	$\frac{21}{2}^+$	744.5(6)	1.7(8)	
		$\frac{19}{2}^+$	1145(1)	2.9(7)	
4304(1)	$(\frac{25}{2}^+)$	$\frac{21}{2}^+$	1175.2(8)	10(2)[c]	
5120(1)	$(\frac{27}{2}^+)$	$(\frac{23}{2}^+)$	1247(1)	1.8(9)	
5479(1)	$(\frac{29}{2}^+)$	$(\frac{25}{2}^+)$	1175.2(8)	10(2)[c]	
6468(2)	$(\frac{31}{2}^+)$	$(\frac{27}{2}^+)$	1348(1)	0.8(3)	
6734(2)	$(\frac{33}{2}^+)$	$(\frac{29}{2}^+)$	1255(1)	2.7(5)	
7992(2)	$(\frac{35}{2}^+)$	$(\frac{31}{2}^+)$	1523(2)	0.6(3)	
8175(2)	$(\frac{37}{2}^+)$	$(\frac{33}{2}^+)$	1441(1)	1.4(6)	
		$[301]\frac{3}{2}^-$ Band			
159.1(1)	$\frac{5}{2}^-$	$\frac{3}{2}^-$	159.1(1)	100(3)[d]	0.55(8)
380.7(2)	$\frac{7}{2}^-$	$\frac{5}{2}^-$	221.6(1)	54(1)	0.46(5)
		$\frac{3}{2}^-$	380.7(2)	13(3)	1.22(28)
648.7(2)	$\frac{9}{2}^-$	$\frac{7}{2}^-$	268.0(1)	25.4(9)	0.48(10)
		$\frac{5}{2}^-$	489.6(2)	18(4)	
981.8(3)	$\frac{11}{2}^-$	$\frac{9}{2}^-$	333.1(2)	13.5(7)	0.45(7)
		$\frac{7}{2}^-$	601.1(3)	17(2)	1.33(16)
1338.8(3)	$\frac{13}{2}^-$	$\frac{11}{2}^-$	357.0(3)	9.6(7)	0.35(3)
		$\frac{9}{2}^-$	690.1(2)	19(1)	0.84(8)
1772.7(4)	$\frac{15}{2}^-$	$\frac{13}{2}^-$	433.9(3)	5.8(9)	0.42(8)
		$\frac{11}{2}^-$	790.9(3)	16(2)	0.81(10)
2201.6(5)	$\frac{17}{2}^-$	$\frac{15}{2}^-$	428.9(4)	4.7(5)	0.54(12)
		$\frac{13}{2}^-$	862.8(4)	14(1)	
2727.5(7)	$\frac{19}{2}^-$	$\frac{17}{2}^-$	525.9(7)	2.5(4)	0.28(12)
		$\frac{15}{2}^-$	954.8(4)	10(1)	1.33(16)
3214.2(9)	$(\frac{21}{2}^-)$	$\frac{19}{2}^-$	486.7(5)	1.6(6)	
		$\frac{17}{2}^-$	1012.6(8)	9(2)	
3831(1)	$(\frac{23}{2}^-)$	$(\frac{21}{2}^-)$	616.7(6)	1.3(7)	
		$\frac{19}{2}^-$	1103(1)	5(1)	
4367(1)	$(\frac{25}{2}^-)$	$(\frac{23}{2}^-)$	535.9(5)	0.7(3)	
		$(\frac{21}{2}^-)$	1153(1)	5(3)	
5085(1)	$(\frac{27}{2}^-)$	$(\frac{23}{2}^-)$	1254(1)	4(1)	
5670(2)	$(\frac{29}{2}^-)$	$(\frac{25}{2}^-)$	1303(1)	3(1)	
7138(2)	$(\frac{33}{2}^-)$	$(\frac{29}{2}^-)$	1468(2)	0.7(4)	
		$[431]\frac{1}{2}^+$ Band			
374.8(3)	$\frac{1}{2}^{(+)}$	$\frac{3}{2}^-$	374.8(3)	>3	0.66(8)
442.7(3)	$\frac{3}{2}^{(+)}$	$\frac{5}{2}^+$	265.5(3)	1.3(5)	0.68(9)
		$\frac{5}{2}^-$	283.6(2)	>5	0.61(7)
597.0(4)	$\frac{5}{2}^{(+)}$	$\frac{3}{2}^{(+)}$	154.3(2)	2.3(3)	
		$\frac{7}{2}^-$	216.3(3)	1.3(3)	0.59(5)
		$\frac{1}{2}^{(+)}$	222.2(2)	5.0(8)	0.92(12)
		$\frac{5}{2}^+$	419.8(4)	0.5(2)	
		$\frac{5}{2}^-$	437.9(4)	1.0(3)	
750.1(5)	$\frac{7}{2}^{(+)}$	$\frac{5}{2}^{(+)}$	153.1(3)	0.7(3)	
		$\frac{3}{2}^{(+)}$	307.4(3)	12(2)	1.11(14)
1031.7(5)	$\frac{9}{2}^{(+)}$	$\frac{7}{2}^{(+)}$	281.6(3)	1.1(4)	0.45(6)
		$\frac{5}{2}^{(+)}$	434.7(3)	8(2)	1.10(19)
1264.4(6)	$\frac{11}{2}^{(+)}$	$\frac{9}{2}^{(+)}$	232.7(4)	0.2(1)	
		$\frac{7}{2}^{(+)}$	514.3(4)	10(3)	1.08(16)
1675.3(6)	$\frac{13}{2}^{(+)}$	$\frac{11}{2}^{(+)}$	410.9(4)	1.0(5)	
		$\frac{9}{2}^{(+)}$	643.6(3)	8(1)	0.97(12)
1980.2(8)	$\frac{15}{2}^{(+)}$	$\frac{13}{2}^{(+)}$	304.9(6)	0.2(1)	
		$\frac{11}{2}^{(+)}$	715.8(4)	9(1)	0.93(22)
2505.8(9)	$(\frac{17}{2}^+)$	$\frac{15}{2}^{(+)}$	525.6(6)	0.3(2)	
		$\frac{13}{2}^{(+)}$	830.5(4)	6(2)	
2887.9(9)	$(\frac{19}{2}^+)$	$\frac{15}{2}^{(+)}$	907.7(4)	7(2)	
3507(1)	$(\frac{21}{2}^+)$	$(\frac{17}{2}^+)$	1001.6(4)	4(2)	
3977(1)	$(\frac{23}{2}^+)$	$(\frac{19}{2}^+)$	1088.8(5)	6(2)	
4667(1)	$(\frac{25}{2}^+)$	$(\frac{21}{2}^+)$	1159(1)	2.2(8)	
5240(1)	$(\frac{27}{2}^+)$	$(\frac{23}{2}^+)$	1264(1)	2(1)	
5974(2)	$(\frac{29}{2}^+)$	$(\frac{25}{2}^+)$	1308(1)	0.8(4)	
6676(2)	$(\frac{31}{2}^+)$	$(\frac{27}{2}^+)$	1436(2)	0.8(4)	

[a]Determined by gating on one or more stretched $E2$ transitions.
[b]From Ref. [8].
[c]Intensity of the 1175-keV doublet.
[d]Intensity normalization.

reduced χ^2 when compared to the experimental spectrum was taken as the lifetime of that state. The uncertainty in the individual lifetimes measured at both angles was determined by finding the lifetime value above and below the best-fit value which increased the minimum reduced χ^2 value by one unit. The accepted lifetime values were determined from a weighted

average (based on the measured uncertainty) of the individual lifetimes measured at both angles (see Table II). In some cases, this weighted average included contributions from a line-shape analysis of both an $M1/E2$ and a stretched $E2$ transition from the same initial state, resulting in the possibility of up to four independent measurements in the determination of the lifetime of a given state. The uncertainties in the accepted lifetimes were deduced from either the standard deviation of the set of individual lifetimes or the smallest uncertainty in the individual lifetime fits, whichever was larger.

Effective lifetimes, which do not include feeding corrections, were first determined for each line shape with adequate statistics. All line shapes were then refit with feeding corrections, with the exception of those from the highest fitted transition in each band, where only the upper-limit effective lifetime could be obtained. The feeding corrections used the effective lifetime of the state (or possibly multiple states) immediately above and one side-feeding state to feed the state of interest. A comparison of fits to the 999 keV ($[422]\frac{5}{2}^+$ band transition) line shape with (mean lifetime) and without (effective lifetime) feeding corrections is shown in Fig. 2 for spectra measured at both 35° and 145°.

Whenever possible, mean lifetimes were determined from spectra gated from above (GFA) the transitions of interest, eliminating the effects of side feeding. In these cases, the transitions were also gated from below (GFB) for the determination of side-feeding times and as a test of consistency. When performing a GFB fit, the total side-feeding intensities

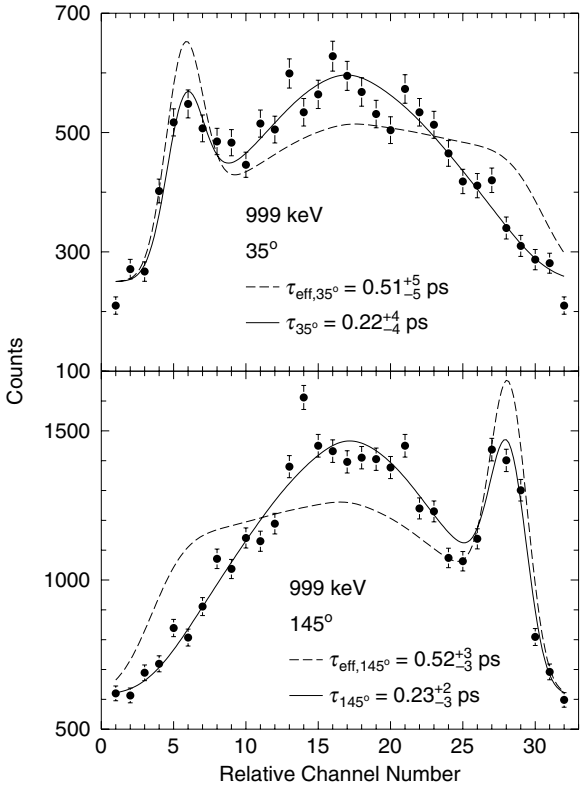

FIG. 2. Fits to the 35° and 145° line shapes of the 999-keV transition in the $[422]\frac{5}{2}^+$ band with (solid line) and without (dashed line) feeding corrections.

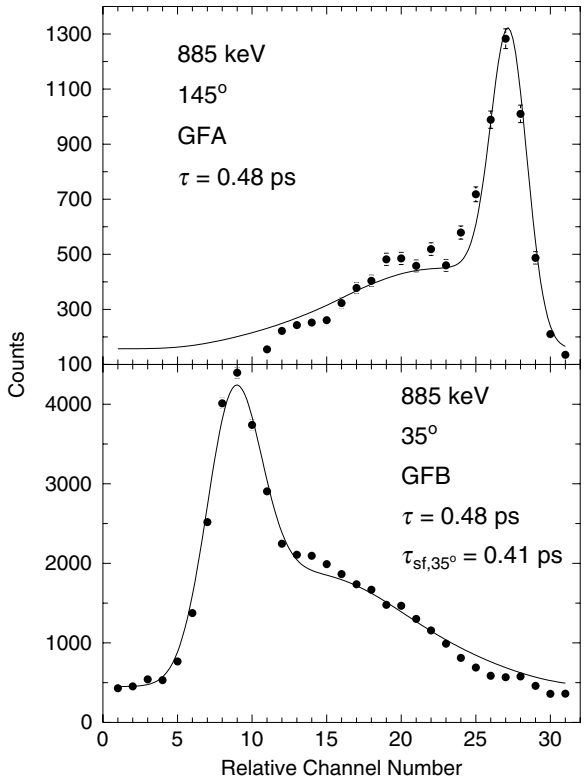

FIG. 3. Fits to the line shape of the 885-keV transition in the $[422]\frac{5}{2}^+$ band gated from above (GFA) at 145° and gated from below (GFB) at 35°. A side-feeding time of 0.41 ps was measured for the $\frac{17}{2}^+$ state from an analysis of the 35° GFB line shape of this transition.

were obtained from the intensity balance of each state, and the side-feeding time was allowed to vary while holding the mean lifetime constant at the value obtained from the GFA result. The side-feeding time which generated a theoretical line shape that had the lowest reduced χ^2 when compared to the experimental GFB spectrum was taken as the side-feeding time of that state. The uncertainty in the side-feeding times were determined in the same way as that described above for the mean lifetime fits. Figure 3 shows a GFA and a GFB fit to the 885-keV transition in the $[422]\frac{5}{2}^+$ band.

Limited statistics often forced the use of only a GFB fit to an experimental line shape. In these situations, the side-feeding times were generally not known but were estimated for the feeding corrections based on the results of a least-squares fit to the measured side-feeding times in both the yrast positive- and negative-parity bands ($[422]\frac{5}{2}^+$ and $[301]\frac{3}{2}^-$ bands in Fig. 1). An exponential function of spin was used since this curve represented the trend of the measured values well and extrapolated to values at the highest observed spins ($\tau_{sf} \sim 0.01$ ps) that were consistent with those used in other recent studies of nuclei in this mass region (see, for example, Refs. [17–19]). This choice is also consistent with the findings of a theoretical study of side-feeding times in this mass region [20], as well as the measured results from ^{82}Sr [21] and ^{83}Y [22]. In many cases, however, the resulting mean lifetimes were rather insensitive to the side-feeding time as long as the side-feeding intensity was small.

TABLE II. Effective lifetimes, mean lifetimes, and side-feeding times measured for states labeled as I_i^π in ^{79}Sr. Individual mean lifetimes deduced from a DSAM analysis of line shapes measured at the indicated angles from transitions with energy E_γ are shown. The effective lifetimes (τ_{eff}) and accepted mean lifetimes (τ_{acc}) represent the weighted average (based on the uncertainties) of the measurements at 35° and 145° where results are available. The accepted side-feeding times ($\tau_{\text{sf,acc}}$) represent the weighted average (based on the uncertainties) of the values measured in this work (τ_{sf}) and those given in a previous study ($\tau_{\text{sf,prev}}$) [8] when both sources are available.

I_i^π	E_γ (keV)	τ_{prev}[a] (ps)	τ_{eff} (ps)	τ_{35°[b] (ps)	τ_{145°[b] (ps)	τ_{acc} (ps)	$\tau_{\text{sf,prev}}$[c] (ps)	τ_{sf} (ps)	$\tau_{\text{sf,acc}}$ (ps)
				$[422]\frac{5}{2}^+$ Band					
$\frac{5}{2}^+$	177	29(1) ns[d]				29(1) ns			
$\frac{7}{2}^+$	152	154(9)				154(9)			
$\frac{9}{2}^+$	169	44(5)				44(5)			
$\frac{11}{2}^+$	415	2.6(3)				2.6(3)	0.5(2)		0.5(2)
$\frac{13}{2}^+$	265	1.7(3)	5.0(27)		1.38^{+132}_{-49}[e]	1.83^{+77}_{-62}	0.4(2)		0.4(2)
	680			1.62^{+77}_{-42}[e]	2.56^{+113}_{-61}[e]				
$\frac{15}{2}^+$	550	<1.0	1.42^{+13}_{-10}	0.50^{+48}_{-21}[e]	0.46^{+26}_{-15}[e]	0.46^{+26}_{-15}		0.43^{+15}_{-11}	0.43^{+15}_{-11}
	815			0.44^{+34}_{-18}[e]					
$\frac{17}{2}^+$	335	0.69^{+7}_{-10}	1.35(25)		0.49^{+22}_{-14}[e]	0.48(6)	0.25^{+25}_{-10}	0.32(11)	0.29(11)
	885			0.46^{+11}_{-9}[e]	0.48(6)[e]				
$\frac{19}{2}^+$	999		0.52(3)	0.22(4)	0.23^{+2}_{-3}	0.23^{+2}_{-3}		0.15[f]	0.15[f]
$\frac{21}{2}^+$	400	0.52(10)	0.53(5)		0.27^{+3}_{-2}	0.23(3)	0.15^{+20}_{-10}	0.10[f]	0.15^{+20}_{-10}
	1065			0.24(2)	0.21^{+2}_{-1}				
$(\frac{23}{2}^+)$	1145		0.33^{+5}_{-4}	0.15^{+5}_{-4}	0.20(3)	0.18(4)		0.07[g]	0.07[g]
$(\frac{25}{2}^+)$	1175	<0.30[h]	0.33(3)			<0.33[h]			
$(\frac{27}{2}^+)$	1247		0.27(10)	0.28^{+10}_{-8}	0.05(2)	0.09^{+16}_{-6}		0.03[g]	0.03[g]
$(\frac{29}{2}^+)$	1175		0.33(3)			<0.33[h]			
$(\frac{31}{2}^+)$	1348		0.14^{+9}_{-5}		0.09^{+8}_{-5}	0.09^{+8}_{-5}		0.02[g]	0.02[g]
$(\frac{33}{2}^+)$	1255		0.23(5)	0.17(4)	0.08(2)	0.10(5)		0.01[g]	0.01[g]
$(\frac{35}{2}^+)$	1523		0.04^{+4}_{-3}			<0.04[h]			
$(\frac{37}{2}^+)$	1441		0.11(4)			<0.11[h]			
				$[301]\frac{3}{2}^-$ Band					
$\frac{5}{2}^-$	159	66(9)[i]				66(9)			
$\frac{7}{2}^-$	222	17(3)[i]				17(3)			
$\frac{9}{2}^-$	268	4.7(12)[i]				4.7(12)			
$\frac{11}{2}^-$	333	1.5(2)	5.7(19)	1.16^{+118}_{-43}[e]	1.74^{+143}_{-57}[e]	1.25^{+58}_{-31}	0.5(2)	0.56^{+25}_{-16}	0.53(20)
	601			1.38^{+137}_{-50}[e]	1.02^{+58}_{-31}[e]				
$\frac{13}{2}^-$	357	1.25(20)	4.0(17)	0.92^{+49}_{-26}[e]	1.18^{+70}_{-34}[e]	1.00^{+25}_{-17}	0.4(2)	0.59(27)	0.48(20)
	690			1.06^{+36}_{-23}[e]	0.93^{+25}_{-17}[e]				
$\frac{15}{2}^-$	434	1.4(1)[h]	2.03(37)	0.66^{+62}_{-25}[e]	0.61^{+37}_{-19}[e]	0.62^{+15}_{-12}		0.31(26)	0.31(26)
	791			0.60^{+22}_{-15}[e]	0.62^{+15}_{-12}[e]				
$\frac{17}{2}^-$	863	0.90(15)	0.94(12)	0.39(3)	0.43(2)	0.41(3)	0.25^{+25}_{-10}		0.25^{+25}_{-10}
$\frac{19}{2}^-$	526		0.66(6)	0.32^{+6}_{-5}	0.41(6)	0.31(5)		0.15[f]	0.15[f]
	955			0.31(3)	0.29^{+2}_{-1}				
$(\frac{21}{2}^-)$	487	<0.6[h]	0.49(7)		0.26(6)	0.24(2)		0.10[f]	0.10[f]
	1013			0.24(4)	0.23(2)				
$(\frac{23}{2}^-)$	1103		0.34(3)	0.19^{+5}_{-4}	0.16^{+2}_{-3}	0.17^{+2}_{-3}		0.07[g]	0.07[g]
$(\frac{25}{2}^-)$	1153		0.28^{+3}_{-2}	0.18(5)	0.14^{+3}_{-2}	0.15(3)		0.05[g]	0.05[g]
$(\frac{27}{2}^-)$	1254		0.19(4)			<0.19[h]			
$(\frac{29}{2}^-)$	1303		0.17(5)	0.08^{+4}_{-3}	0.13^{+4}_{-2}	0.11(4)		0.02[g]	0.02[g]
$(\frac{33}{2}^-)$	1468		0.13(4)			<0.13[h]			

TABLE II. *(Continued.)*

I_i^π	E_γ (keV)	τ_{prev}[a] (ps)	τ_{eff} (ps)	τ_{35°[b] (ps)	τ_{145°[b] (ps)	τ_{acc} (ps)	$\tau_{\text{sf,prev}}$[c] (ps)	τ_{sf} (ps)	$\tau_{\text{sf,acc}}$ (ps)
				$[431]\frac{1}{2}^+$ Band					
$\frac{13}{2}^{(+)}$	644		2.83^{+34}_{-27}	1.60^{+150}_{-53}[e]	1.64^{+53}_{-32}[e]	1.63^{+53}_{-32}		0.58^{+190}_{-37}	0.58^{+190}_{-37}
$\frac{15}{2}^{(+)}$	716		1.74(23)		0.94^{+24}_{-15}[e]	0.94^{+24}_{-15}		0.31^{+57}_{-30}	0.31^{+57}_{-30}
$(\frac{17}{2}^+)$	830		0.72(13)	0.44(6)	0.36(3)	0.39(6)		0.21[f]	0.21[f]
$(\frac{19}{2}^+)$	908		0.45^{+3}_{-2}	0.19(4)	0.21^{+3}_{-2}	0.20^{+3}_{-2}		0.15[f]	0.15[f]
$(\frac{21}{2}^+)$	1002		0.33(5)	0.20^{+5}_{-4}	0.23(4)	0.22(4)		0.10[f]	0.10[f]
$(\frac{23}{2}^+)$	1089		0.22(7)	0.16(4)	0.09(2)	0.11(5)		0.07[g]	0.07[g]
$(\frac{25}{2}^+)$	1159		0.16(2)			<0.16[h]			
$(\frac{27}{2}^+)$	1264		0.17(2)	0.08^{+7}_{-4}	0.13(2)	0.12(4)		0.03[g]	0.03[g]
$(\frac{31}{2}^+)$	1436		0.07(4)			<0.07[h]			

[a]From Ref. [8] unless otherwise noted.
[b]Determined from spectra gated from below (GFB) the listed transition, unless otherwise noted.
[c]From Ref. [8].
[d]From Ref. [9].
[e]Determined from spectra gated from above (GFA) the listed transition.
[f]Interpolated value (see text).
[g]Extrapolated value (see text).
[h]Effective lifetime.
[i]From a weighted average (based on the uncertainties) of results in Refs. [8,10].

III. RESULTS

A. The level scheme

The level scheme of ^{79}Sr as deduced from this work is shown in Fig. 1. In general, the decay scheme published most recently [12] has been verified and is in good agreement with the present study, although excited states could not be observed to as high a spin as in that work. The measured γ-ray intensities show generally good agreement with those measured previously [8,9] whenever comparisons were possible.

Although the band labeled $[431]\frac{1}{2}^+$ in Fig. 1 has been incorporated in prior versions of the ^{79}Sr level scheme [11,12], only limited spectroscopic data about this sequence have been published thus far. In this work, several γ-ray intensities and DCO ratios, as well as level lifetimes, have been measured in this band and are given in Tables I and II. The results at least partially confirm the spin assignments and level ordering given in Refs. [11,12]. The tentative assignment of positive parity is based on the strong similarity of this band to a band suggested to be based on the $[431]\frac{1}{2}^+$ configuration in ^{81}Sr [5,6], as well as the successful description of the experimental moments of inertia of this band assuming a $[431]\frac{1}{2}^+$ configuration in projected shell-model calculations [12]. Figure 4 shows an example coincidence spectrum resulting from gating on the 284- and 644-keV γ rays from the decay of the $\frac{3}{2}^{(+)}$ and $\frac{13}{2}^{(+)}$ states in this band, respectively (see Fig. 1).

The 216-keV line that was suggested [12] to be a transition between the $\frac{1}{2}^{(+)}$ state in this band and the $\frac{5}{2}^-$ state in the $[301]\frac{3}{2}^-$ band (see Fig. 3 in Ref. [12]) has been rearranged as a transition from the $\frac{5}{2}^{(+)}$ state in this band to the $\frac{7}{2}^-$ state in the $[301]\frac{3}{2}^-$ band instead (see Fig. 1). This change is supported by observed coincidences between the 216-keV

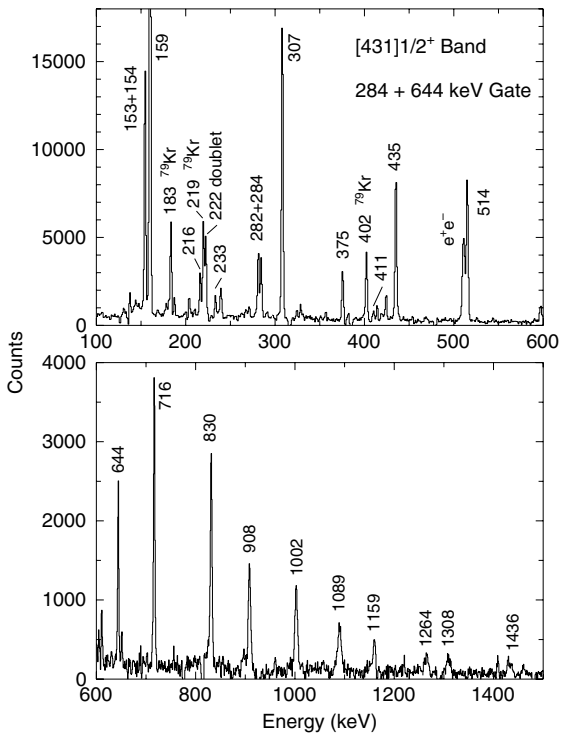

FIG. 4. A portion of the 90° spectrum gated on the 284- and 644-keV transitions showing coincidences with decays in the $[431]\frac{1}{2}^+$ band. The dispersion is 0.9 keV/channel. The ^{79}Kr lines originate from the β^+ decay of ^{79}Rb to ^{79}Kr.

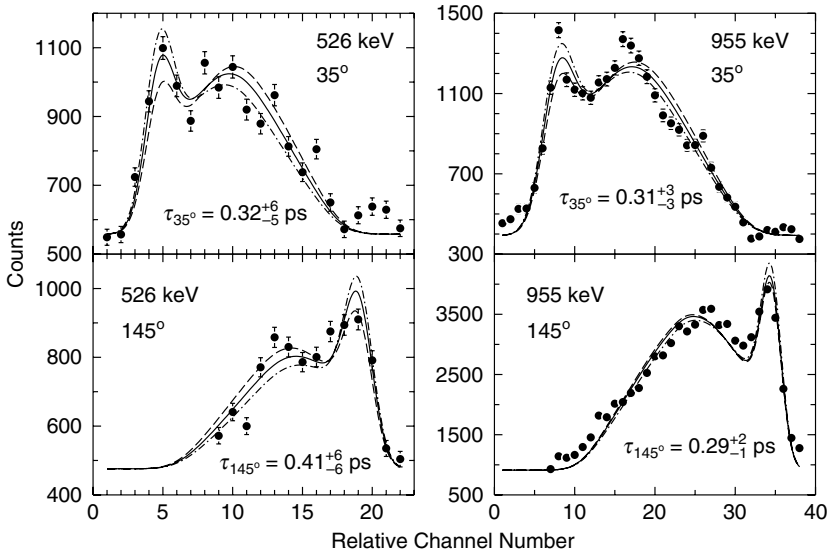

FIG. 5. Fits to the 35° and 145° line shapes of the 526- and 955-keV transitions that decay the same $\frac{19}{2}^-$ state in the $[301]\frac{3}{2}^-$ band. The accepted mean lifetime of the $\frac{19}{2}^-$ state ($\tau_{acc} = 0.31(5)$ ps) was determined from a weighted average (based on the uncertainties) of the individual lifetimes measured from each of these line shapes.

transition and the 381-keV transition in the $[301]\frac{3}{2}^-$ band, as well as the measured DCO ratio of the 216-keV line, which is indicative of a $\Delta I = 1$, rather than a $\Delta I = 2$, transition (see Table I). (The strong observed coincidences between 216- and 222-keV γ rays can still be explained in this new construction, as seen from Fig. 1.) Furthermore, an $M2/E3$ character for the 216-keV transition, as would be the case in the previously suggested placement of this decay, would be highly unlikely to compete with the much stronger 375-keV $E1$ decay from the same $\frac{1}{2}^{(+)}$ state. The new placement of the 216-keV transition assigns an $E1$ multipolarity to this decay, yielding reasonable $B(E1)$ estimates given the likely range of lifetimes for the $\frac{5}{2}^{(+)}$ parent state.

The measured intensities of the 284- and 375-keV transitions from the $\frac{3}{2}^{(+)}$ and $\frac{1}{2}^{(+)}$ states, respectively, of this band were smaller than the intensity balance of each state would suggest. Considering the 100 ns γ-ray coincidence time window used during the experiment, it is therefore likely that the lifetimes of the $\frac{1}{2}^{(+)}$ and $\frac{3}{2}^{(+)}$ states in this band are at least tens of nanoseconds to account for the reduced intensities. This appears to be a systematic trend of other $I = \frac{1}{2}$ and $\frac{3}{2}$ states in bands that are also suggested to be based on the $[431]\frac{1}{2}^+$ configuration in neighboring nuclei. In the $N = 41$ isotone ^{81}Zr, a lower limit of about 40 ns was deduced for the lifetimes of these states [12]. In ^{81}Sr, the lifetimes of the $\frac{1}{2}^{(+)}$ and $\frac{3}{2}^{(+)}$ states were measured [4] to be 35(6) and 0.91(29) ns, respectively. A similar reduction in intensity was also observed for the 177-keV decay from the $\frac{5}{2}^+$ state in the $[422]\frac{5}{2}^+$ band due to the 29-ns mean lifetime of the parent state [9].

B. Lifetime measurements

Lifetimes of 33 excited states were measured using the DSAM and are given in Table II. The effective lifetimes represent the weighted average (based on the individual uncertainties) of the results obtained from each of the two detector angles for which they could be measured. Mean lifetimes, which include feeding corrections, are given for each detector angle along with the accepted lifetime that also represents the weighted average of the results at each angle. Results obtained from a previous DSAM analysis [8] are included for comparison (τ_{prev}). If a reliable line shape could not be obtained at one angle, a lifetime result is not included in the table. Measured side-feeding times (τ_{sf}) are also included in the table along with those given in Ref. [8]. The accepted side-feeding time for a particular state ($\tau_{sf,acc}$) represents the weighted average (based on the individual uncertainties) of the results obtained from this work and those from Ref. [8] if a value was measured from both sources. (If measurements are unavailable, values that were interpolated or extrapolated from the measured ones are given.) Figure 5 shows the four independent line shapes that were used to determine the lifetime of the $\frac{19}{2}^-$ state in the $[301]\frac{3}{2}^-$ band.

1. Positive-parity states

DSAM lifetimes were measured previously [8] in the yrast positive-parity band (labeled $[422]\frac{5}{2}^+$ in Fig. 1) up to the $(\frac{25}{2}^+)$ state, where an effective lifetime of <0.30 ps is given. Still, only an estimate of $\tau < 1.0$ ps was given for the $\frac{15}{2}^+$ state, and a lifetime was not measured for the $\frac{19}{2}^+$ state (see Table II). In this work, most lifetimes between the $\frac{13}{2}^+$ and $(\frac{37}{2}^+)$ states were measured by using either a GFA or GFB analysis (see Table II for the distinction). Line shapes could not be extracted above the $(\frac{37}{2}^+)$ and $(\frac{35}{2}^+)$ levels, so only effective lifetimes are quoted for these states. The measured values for the $\frac{17}{2}^+$ and $\frac{21}{2}^+$ states are significantly smaller than the values measured previously [8] (see Table II). However, the side-feeding time measured for the $\frac{17}{2}^+$ state is in rather good agreement with the value given in Ref. [8], and the interpolated side-feeding time for the $\frac{21}{2}^+$ state based on the exponential curve fit to the measured values was similar to that determined in that study (see Table II). A portion of Fig. 6 shows the fit to the 145° line shape of the 1065-keV decay of the $\frac{21}{2}^+$ state in this band and

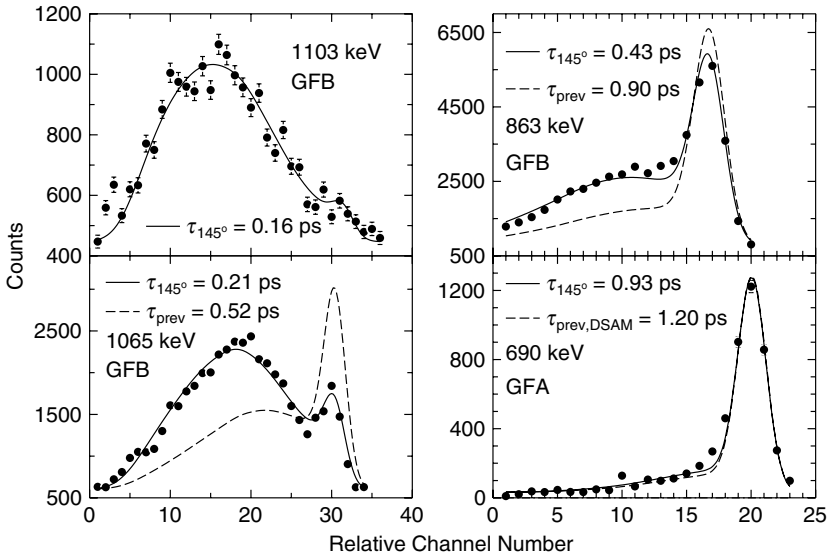

FIG. 6. Fits to the 145° line shapes of four transitions in the $[422]\frac{5}{2}^{+}$ and $[301]\frac{3}{2}^{-}$ bands. The solid curve indicates the best fit to the observed line shapes, while the dashed lines show the line shapes resulting from the mean lifetimes reported from a previous DSAM analysis [8] where data are available. The previous mean lifetime value used for the line shape of the 690-keV transition ($\tau_{prev,DSAM}$) results from only the DSAM analysis performed in Ref. [8] and does not include the contribution of an analysis using the recoil-distance method for the same transition. Line shapes that were generated by gating from above (GFA) and gating from below (GFB) the given transition are also indicated.

how it compares to a theoretical line shape representative of the mean lifetime measured for this state in Ref. [8].

A simultaneous fit was performed to the 1247- and 1255-keV lines to decompose their GFB line shapes and extract lifetimes individually for the $(\frac{27}{2}^{+})$ and $(\frac{33}{2}^{+})$ states, respectively. A modified version of FITS [23] was used to fit the two overlapping line shapes simultaneously, with the theoretical line shapes scaled by the intensity of each transition. It was also possible to obtain a weak, but clean, GFB line shape for the 1255-keV transition at 145° by gating on the 1175-keV doublet. An independent analysis of this line shape gave a lifetime of 0.07(2) ps for the $(\frac{33}{2}^{+})$ state, in good agreement with the result obtained from the simultaneous fit of the combined 1247- and 1255-keV line shapes measured at 145° (see Table II). The statistics were too weak to remeasure the lifetime by this method at 35°. The final accepted lifetime of the $(\frac{33}{2}^{+})$ state (see Table II) incorporated the one independent fit of the 1255-keV line shape as part of a weighted average (based on the measurement uncertainty) of all measurements (see Table II). The individual line shapes that comprise the 1175-keV doublet could not be resolved, and so only effective lifetimes are given for the $(\frac{25}{2}^{+})$ and $(\frac{29}{2}^{+})$ states in Table II.

Nine lifetimes were also measured for the first time in the band labeled $[431]\frac{1}{2}^{+}$ in Fig. 1. Reliable line shapes could not be extracted above the $(\frac{25}{2}^{+})$ and $(\frac{31}{2}^{+})$ states in the $\alpha = +\frac{1}{2}$ and $\alpha = -\frac{1}{2}$ signatures, respectively, and hence only effective lifetimes could be quoted for these levels. While there were adequate statistics to perform a GFA analysis of the line shapes of the 644- and 716-keV transitions, all other line-shape analysis was performed using GFB spectra. Figure 7 shows the fits to the 145° line shapes of the 716-, 908-, and 1089-keV transitions in this band.

2. *Negative-parity states*

DSAM lifetimes were measured previously [8] in the yrast negative-parity band (labeled $[301]\frac{3}{2}^{-}$ in Fig. 1) as high as the $(\frac{21}{2}^{-})$ state, where an effective lifetime of <0.6 ps is given. In this work, lifetimes were measured from the $\frac{11}{2}^{-}$ state to the $(\frac{33}{2}^{-})$ state by using either a GFA or GFB analysis (see Table II for the distinction). Reliable line shapes could not

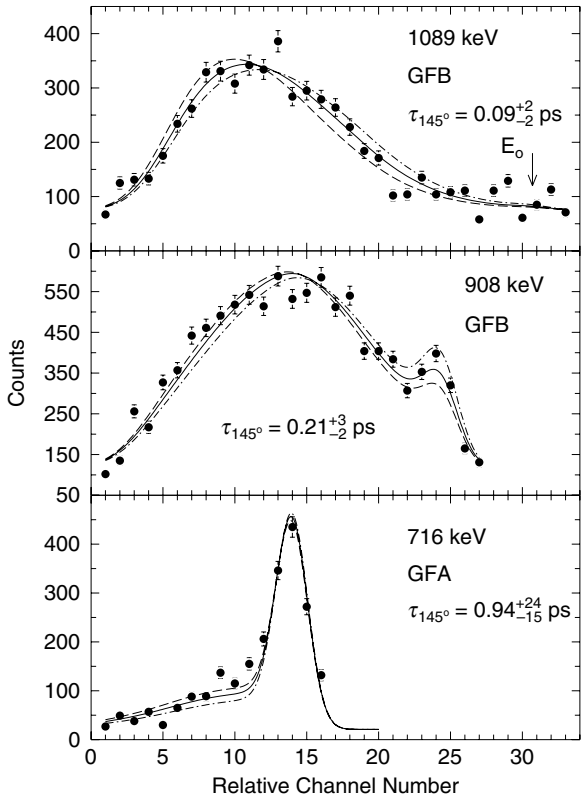

FIG. 7. Fits to the 145° line shapes of the 716-, 908-, and 1089-keV transitions in the $[431]\frac{1}{2}^{+}$ band. The uncertainty limits of the best fit (solid curve) are indicated by the broken curves. The expected position of an unshifted peak near 1089 keV (E_0) is shown by the arrow in the top panel. Line shapes that were generated by gating from above (GFA) and gating from below (GFB) the given transition are also indicated.

be extracted above the $(\frac{33}{2}^-)$ and $(\frac{27}{2}^-)$ states in the $\alpha = +\frac{1}{2}$ and $\alpha = -\frac{1}{2}$ signatures, respectively, and hence only effective lifetimes could be quoted for these levels. As was the case in the yrast positive-parity band, the measured mean lifetime of the spin $I = \frac{17}{2}$ state in this band was significantly smaller than the previous result [8], as shown in Fig. 6 from a comparison of the two line-shape fits to the 863-keV decay. At lower spins, the measured results compare somewhat more favorably with the other DSAM analysis [8] and two separate measurements using the recoil-distance method [8,10] when there is an overlap in the results from the two methods. However, these comparisons should be made with caution since the DSAM technique tends to become less reliable once the mean lifetimes exceed about 1 ps. The rather large uncertainties associated with measured values about 1 ps or larger reflect this. Figure 6 includes the fits to the 145° line shapes of the 690- and 1103-keV transitions in this band as well.

C. Transition strengths

Reduced electric quadrupole transition strengths $B(E2)$ were determined from the accepted lifetimes given in Table II and were used to calculate transition quadrupole moments $|Q_t|$ from the rotational model according to

$$Q_t^2 = \frac{16\pi}{5}\langle I\,K\,20|I-2K\rangle^{-2} B(E2, I \rightarrow I-2). \quad (2)$$

The Q_t values provide a measure of the quadrupole deformation β_2. Assuming axial symmetry, β_2 is determined approximately by

$$\beta_2 = \sqrt{\frac{49\pi}{80} + \frac{7\pi\, Q_t}{6eZr_0^2A^{2/3}}} - \sqrt{\frac{49\pi}{80}}. \quad (3)$$

For the purpose of discussion, β_2 values have been inferred from the Q_t values using $r_0 = 1.2$ fm. The $B(E2)$, Q_t, and β_2 values are given in Table III. Some of these values included in the table were deduced from two separate lifetime measurements using the recoil-distance method [8,10] for completeness.

Magnetic dipole transition strengths $B(M1)$ were calculated for $\Delta I = 1$ transitions in the yrast positive- and negative-parity bands using the measured quadrupole-dipole mixing ratios δ given in Refs. [1,8]. When a value of δ was not available for a particular transition in these bands, an average value determined from the measured values in the same band was used. $B(M1)$ strengths were also estimated for $\Delta I = 1$ transitions in the $[431]\frac{1}{2}^+$ band of Fig. 1 by assuming a value of $\delta = 0$ since $B(M1)$ values are rather insensitive to δ as long as it is small. (For example, varying δ from zero to an average value of $\delta_{\rm ave} = -0.19(9)$, indicative of all measured values in ^{79}Sr, changes the $B(M1)$ values by less than 5%, well within the measured uncertainties.) At any rate, these $B(M1)$ estimates can be considered upper limits for the transitions in this band. All deduced $B(M1)$ strengths are included in Table III.

IV. DISCUSSION

Previous cranked-shell model (CSM) analyses of the yrast positive- and negative-parity bands in ^{79}Sr [8,9], based on the $[422]\frac{5}{2}^+$ and $[301]\frac{3}{2}^-$ bandhead configurations, revealed very different behaviors between these two structures as a function of rotational frequency. The $[422]\frac{5}{2}^+$ band showed a sharp alignment near a rotational frequency $\hbar\omega \approx 0.58$ MeV, while in contrast the $[301]\frac{3}{2}^-$ band was observed to have only a very gradual alignment. Although both band crossings were attributed [8,9] to a $g_{9/2}$ proton alignment, the alignment in the $[422]\frac{5}{2}^+$ band was associated with a change in shape from prolate ($\gamma = 0°$) at low spin to (modestly) triaxial ($\gamma \approx -10°$) that begins just below the band crossing and continues to higher spin, while the observed alignment in the $[301]\frac{3}{2}^-$ band was determined to be consistent with a picture of an axially deformed rotor both above and below the band-crossing region [9]. These conclusions were supported by the predictions of cranked Woods-Saxon (CWS) calculations, which also indicated a reduction in collectivity in the band-crossing region [8,9]. Lifetime measurements [8] provided confirmation of a reduction in $B(E2)$ strengths in the band-crossing regions of both bands, but were not extended to higher spins to see if this pattern continued.

A more recent investigation [12] confirmed these findings through another CSM analysis, which was compared to the predictions of the projected shell model (PSM) [13]. Both yrast structures were observed to higher spins and thus the possibility of additional alignments at higher frequencies were explored. Although the $[422]\frac{5}{2}^+$ band showed no further evidence of additional structure changes, the $[301]\frac{3}{2}^-$ band displayed a pronounced alignment near $\hbar\omega = 0.8$ MeV, in good agreement with the expectation of a $g_{9/2}$ neutron alignment near this frequency based on calculations of quasineutron Routhians assuming a suitable shape for this configuration [8]. The work of Ref. [12] also provided a high-spin analysis of a band based on the $[431]\frac{1}{2}^+$ orbital, showing perhaps a gradual alignment similar to the one observed in the $[301]\frac{3}{2}^-$ band.

The lifetimes measured in this work through and above the band-crossing regions in both the $[422]\frac{5}{2}^+$ and $[301]\frac{3}{2}^-$ bands, as well as in the $[431]\frac{1}{2}^+$ band for the first time, allow for a direct test of the interpretations of both the CSM and CWS analyses at high spin through a study of the behavior of the resulting transition quadrupole moments Q_t. The results are discussed separately below, along with their interpretation within the context of additional CWS and PSM calculations.

A. Projected shell-model calculations

Calculations have been performed within the context of the PSM [13] to investigate further the collective properties of the three observed band structures in ^{79}Sr. Previous calculations using the PSM applied to ^{79}Sr [12] reproduced nicely the gradual alignments observed in the $[301]\frac{3}{2}^-$ and $[431]\frac{1}{2}^+$ bands, but could not describe the sharp alignment in the $[422]\frac{5}{2}^+$ band (see Fig. 5 in Ref. [12]). At that time, predictions

TABLE III. Spins, γ-ray energies, branching ratios R_B, electric quadrupole transition strengths $B(E2)$, magnetic dipole transition strengths $B(M1)$, transition quadrupole moments $|Q_t|$, and quadrupole deformations β_2 in ^{79}Sr.

I_i^π	E_γ (keV)	R_B(%)	$B(E2)$ (W.u.)[a,b]	$B(M1)$ (μ_N^2)[b]	$\lvert Q_t\rvert$ (eb)	β_2[c]
			$[422]\frac{5}{2}^+$ Band			
$\frac{5}{2}^+$	177	100		$3.24(11)\times10^{-6}$[d]		
$\frac{7}{2}^+$	152	100	148^{+117}_{-87}	0.100^{+7}_{-6}		
$\frac{9}{2}^+$	321	21	57^{+7}_{-6}		3.40^{+21}_{-18}	0.39(2)
	169	79	333^{+161}_{-135}	0.20^{+3}_{-2}		
$\frac{11}{2}^+$	584	29	67^{+9}_{-7}		2.82^{+18}_{-15}	0.33(2)
	415	71	108^{+90}_{-71}	0.19(3)		
$\frac{13}{2}^+$	680	78	120^{+61}_{-35}		3.35^{+77}_{-54}	0.39^{+7}_{-6}
	265	22	115^{+162}_{-86}	0.35^{+18}_{-10}		
$\frac{15}{2}^+$	815	64	157^{+76}_{-57}		3.59^{+78}_{-72}	0.41^{+8}_{-7}
	550	36		0.25^{+12}_{-9}		
$\frac{17}{2}^+$	885	86	134^{+19}_{-15}		3.17^{+22}_{-18}	0.37(2)
	335	14		0.41^{+6}_{-5}		
$\frac{19}{2}^+$	999	64	114^{+17}_{-9}		2.84^{+21}_{-12}	0.33^{+2}_{-1}
	664	36		0.28^{+4}_{-2}		
$\frac{21}{2}^+$	1065	87	112^{+17}_{-13}		2.76^{+20}_{-16}	0.32^{+3}_{-1}
	400	13		0.46^{+7}_{-6}		
$(\frac{23}{2}^+)$	1145	63	72^{+21}_{-13}		2.18^{+29}_{-21}	0.26^{+3}_{-2}
	744	37		0.27^{+8}_{-5}		
$(\frac{25}{2}^+)$	1175	100	>55[e]		>1.87[e]	>0.23[e]
$(\frac{27}{2}^+)$	1247	100	149^{+299}_{-96}		3.06^{+224}_{-123}	0.36^{+22}_{-14}
$(\frac{29}{2}^+)$	1175	100	>55[e]		>1.84[e]	>0.22[e]
$(\frac{31}{2}^+)$	1348	100	101^{+127}_{-48}		2.48^{+124}_{-68}	0.29^{+13}_{-7}
$(\frac{33}{2}^+)$	1255	100	130^{+130}_{-43}		2.80^{+116}_{-51}	0.33^{+12}_{-6}
$(\frac{35}{2}^+)$	1523	100	>124[e]		>2.72[e]	>0.32[e]
$(\frac{37}{2}^+)$	1441	100	>59[e]		>1.88[e]	>0.23[e]
			$[301]\frac{3}{2}^-$ Band			
$\frac{5}{2}^-$	159	100	48^{+84}_{-43}	0.21^{+3}_{-2}		
$\frac{7}{2}^-$	381	19	56^{+12}_{-8}		2.82^{+29}_{-22}	0.33^{+3}_{-2}
	222	81	102^{+98}_{-68}	0.24^{+5}_{-4}		
$\frac{9}{2}^-$	490	41	126^{+43}_{-25}		3.45^{+54}_{-37}	0.40^{+5}_{-4}
	268	59	60^{+69}_{-44}	0.36^{+12}_{-7}		
$\frac{11}{2}^-$	601	56	230^{+76}_{-73}		4.28^{+65}_{-74}	0.48^{+6}_{-8}
	333	44	191^{+117}_{-101}	0.52^{+17}_{-16}		
$\frac{13}{2}^-$	690	66	172^{+35}_{-34}		3.53^{+34}_{-37}	0.40^{+4}_{-3}
	357	34	11^{+34}_{-11}	0.42^{+9}_{-8}		
$\frac{15}{2}^-$	791	73	154^{+37}_{-30}		3.24^{+37}_{-33}	0.37^{+4}_{-3}
	434	27	25^{+20}_{-15}	0.30^{+7}_{-6}		
$\frac{17}{2}^-$	863	75	155^{+12}_{-11}		3.19^{+12}_{-11}	0.37(1)
	429	25		0.43^{+4}_{-3}		
$\frac{19}{2}^-$	955	80	132^{+25}_{-18}		2.89^{+27}_{-21}	0.34^{+3}_{-2}
	526	20		0.25^{+5}_{-4}		
$(\frac{21}{2}^-)$	1013	84	134^{+12}_{-10}		2.89^{+13}_{-11}	0.34(1)
	487	16		0.32^{+3}_{-2}		
$(\frac{23}{2}^-)$	1103	80	116^{+25}_{-12}		2.67^{+27}_{-14}	0.31^{+3}_{-1}
	617	20		0.28^{+6}_{-3}		

TABLE III. *(Continued.)*

I_i^π	E_γ (keV)	R_B (%)	$B(E2)$ (W.u.)[a,b]	$B(M1)$ (μ_N^2)[b]	$\lvert Q_t \rvert$ (eb)	β_2[c]
$(\frac{25}{2}^-)$	1153	88	117^{+29}_{-20}		2.66^{+31}_{-23}	0.31^{+4}_{-2}
	536	12		0.29^{+7}_{-5}		
$(\frac{27}{2}^-)$	1254	100	>69[e]		>2.03[e]	>0.24[e]
$(\frac{29}{2}^-)$	1303	100	98^{+56}_{-26}		2.41^{+61}_{-35}	0.29^{+6}_{-4}
$(\frac{33}{2}^-)$	1468	100	>46[e]		>1.63[e]	>0.20[e]
			$[431]\frac{1}{2}^+$ Band			
$\frac{13}{2}^{(+)}$	644	89	201(49)		3.60^{+42}_{-47}	0.41^{+4}_{-5}
	411	11		0.05(1)		
$\frac{15}{2}^{(+)}$	716	98	226^{+43}_{-46}		3.76^{+34}_{-40}	0.43^{+3}_{-4}
	305	2		0.04(1)		
$(\frac{17}{2}^+)$	830	95	249^{+45}_{-33}		3.91^{+34}_{-27}	0.44^{+4}_{-2}
	526	5		0.05(1)		
$(\frac{19}{2}^+)$	908	100	329^{+37}_{-43}		4.46^{+24}_{-30}	0.50^{+2}_{-3}
$(\frac{21}{2}^+)$	1002	100	183^{+41}_{-28}		3.31^{+35}_{-27}	0.38^{+4}_{-3}
$(\frac{23}{2}^+)$	1089	100	241^{+201}_{-75}		3.78^{+134}_{-65}	0.43^{+13}_{-7}
$(\frac{25}{2}^+)$	1159	100	>121[e]		>2.67[e]	>0.31[e]
$(\frac{27}{2}^+)$	1264	100	105^{+52}_{-26}		2.47^{+56}_{-33}	0.29^{+6}_{-3}
$(\frac{31}{2}^+)$	1436	100	>95[e]		>2.34[e]	>0.28[e]

[a] 1 W.u. $= 20.1\ e^2\text{fm}^4$.
[b] See text for a discussion of the quadrupole-dipole mixing ratio δ used for $M1/E2$ transitions.
[c] Assuming axial symmetry.
[d] $B(E1)$ in W.u., assuming $\delta = 0$. 1 W.u. $= 1.18\ e^2\text{fm}^2$.
[e] Based on an effective lifetime value.

on the degree of collectivity as a function of spin were not given since no new lifetime information was available at high spin.

The PSM uses a rotational-invariant Hamiltonian, including quadrupole-quadrupole, monopole-pairing, and quadrupole-pairing interaction terms. The strength of the quadrupole-quadrupole force was chosen so that the self-consistent relation with the input deformation parameter is kept. The monopole-pairing force strength took the form

$$G_M = \left[G_1 - G_2 \frac{N-Z}{A} \right] A^{-1}, \tag{4}$$

where $G_1 = 20.25$ for both neutrons and protons, and $G_2 = 16.20$ (0) for neutrons (protons). The quadrupole-pairing strength, assumed to be proportional to the monopole strength, was 16% of the monopole-pairing strength. These strengths are the same as those employed in previous PSM calculations for this mass region [12,24–26].

In the calculations, the deformed quasiparticle (qp) basis is constructed from the Nilsson single-particle states followed by a BCS calculation. The single-particle space includes all nucleons in the $N = 2, 3, 4$ major shells. To build the shell-model basis for a nucleus with an odd number of neutrons, the quasineutron creation operator is applied to the qp-vacuum state, and the resulting set of 1–qp states are projected onto good angular-momentum states. (The one-quasineutron states include, among others, the $[422]\frac{5}{2}^+$, $[301]\frac{3}{2}^-$, and $[431]\frac{1}{2}^+$ orbitals that lie near the Fermi level.) In addition, the shell-model basis includes projected 3-qp states that are built by these one-quasineutron states plus a $g_{9/2}$ proton pair. We expect that mixing of the configurations with 1-qp and 3-qp states at appropriate spins describes the rotation alignment of $g_{9/2}$ protons. The projected basis is used to diagonalize the shell-model Hamiltonian. The resulting eigenstates (wave functions) are used to determine transition strengths [27], and the $B(E2)$ strengths are used to calculate transition quadrupole moments according to Eq. (2). The shell-model bases were constructed using a deformation parameter of $\epsilon_2 = 0.36$ to remain consistent with the previous PSM results for ^{79}Sr [12]. More details about the PSM calculations specific to this work can be found in Ref. [12]. Comparisons between the PSM predictions for ^{79}Sr and the measured results are discussed separately for each band in the sections that follow.

B. Cranked Woods-Saxon calculations

The evolution of shape and deformation with rotational frequency has been studied previously [8,9] for the $[422]\frac{5}{2}^+$ and $[301]\frac{3}{2}^-$ bands using the CWS approach [3]. Similar calculations have been performed in this work in order to attempt to illuminate the structural characteristics of the $[431]\frac{1}{2}^+$ band.

The calculations generate a total Routhian surface (TRS) plot in the (β_2, γ) plane at discrete rotational frequencies, using a deformed Woods-Saxon potential and a short-range monopole pairing force [3]. At each grid point, the

Routhian was minimized with respect to the hexadecapole deformation β_4.

To estimate the deformation of the $[431]\frac{1}{2}^+$ band as a function of rotational frequency (or spin) using this model, calculations were performed using nonyrast intrinsic configurations having positive parity. Using the quasiparticle labeling scheme of Ref. [28], where upper case letters are used for 1-qp neutron configurations, the D (and signature partner C) configuration was used as a possible candidate to represent this band. Although this choice does not represent an unambiguous assignment to the $d_{5/2}$ orbital because of Coriolis mixing at high spin with the $g_{9/2}$ orbital, it does represent the lowest-energy 1-qp configuration for nonyrast positive-parity states available in the calculations.

Figure 8 shows two representative TRS plots resulting from the calculations performed at two rotational frequencies (and their corresponding spins). Large deformations near $\beta_2 = 0.4$ are indicated near the prolate-deformed axis at $\gamma = 0^\circ$ at both frequencies, indicating a near-prolate shape that remains mostly rigid in nature over at least part of the range of spins in which lifetimes were measured in this work. Comparisons between the deformations predicted by these calculations and those implied from the lifetime measurements are discussed in Sec. IV E.

Theoretical Q_t values were calculated for each band in which lifetimes were measured by using the β_2 values obtained from the TRS plots. To make a proper comparison between experimental and theoretical values, the quadrupole deformation of the nuclear matter distribution derived from the TRS calculations was first related to the charge quadrupole deformation derived from the $B(E2)$ strengths [29,30]. To take triaxiality into account, the high-spin limit for the γ dependence of Q_t [31,32] was used to determine the accepted theoretical Q_t values from those calculated assuming axial symmetry [29]. Comparisons between the Q_t values predicted by the CWS calculations and those obtained experimentally are discussed separately for each band in the following sections.

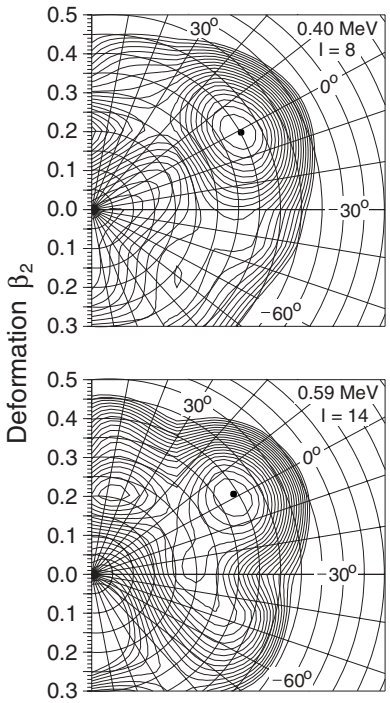

FIG. 8. Sample total Routhian surface plots for an intrinsic configuration that most likely represents the $[431]\frac{1}{2}^+$ band in ^{79}Sr, representative of the results obtained within the range of spins in which lifetimes were measured in this work. The rotational frequency and corresponding spin I are shown in each plot. The spacing between contour lines is 200 keV.

C. $[422]\frac{5}{2}^+$ band

The transition quadrupole moments Q_t deduced from the measured lifetimes in the $[422]\frac{5}{2}^+$ band are shown in the top panel of Fig. 9. The results imply rather large collectivity and deformation over a wide range of spins, corresponding to an average quadrupole deformation $\beta_{2,\mathrm{ave}} = 0.34$, assuming axial symmetry. These values are generally in fair agreement with the predictions of CWS and PSM calculations, as shown by the curves in the same figure, although the agreement with the PSM predictions is systematically better. A clear reduction in

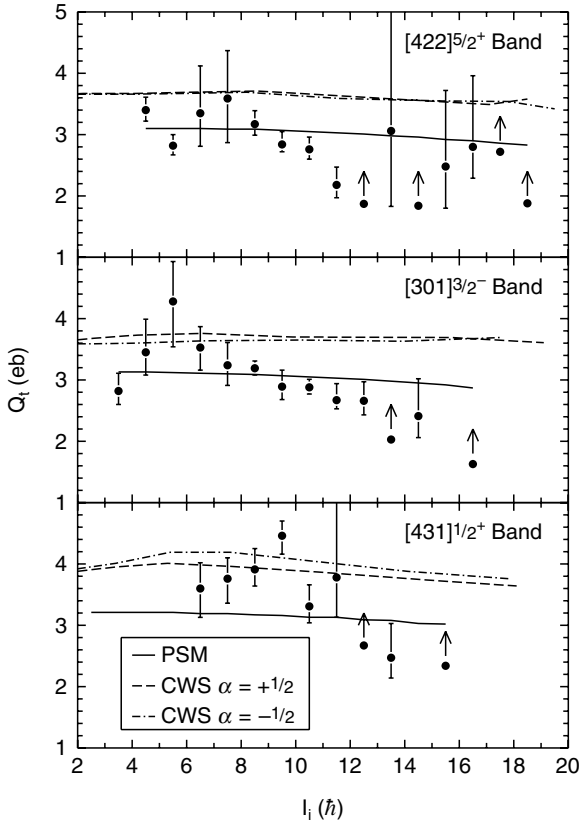

FIG. 9. Transition quadrupole moments Q_t as a function of the initial-state spin I_i for the $[422]\frac{5}{2}^+$ (top), $[301]\frac{3}{2}^-$ (middle), and $[431]\frac{1}{2}^+$ (bottom) bands in ^{79}Sr. Symbols with arrows indicate lower limits established from effective lifetime measurements. The curves represent theoretical predictions from the projected shell-model (PSM) and cranked Woods-Saxon (CWS) calculations, as indicated in the figure.

Q_t, consistent within experimental uncertainty, occurs at the $(\frac{23}{2}^+)$ state, soon before a sharp $g_{9/2}$ proton alignment occurs near the $(\frac{25}{2}^+)$ state [8,9]. The spin at which this decrease in Q_t occurs is somewhat larger than that observed in an earlier study [8], but this can be attributed to a comparatively shorter lifetime measured for the $\frac{21}{2}^+$ state in this work. Qualitatively, the drop is similar and could be correlated to the onset of the proton alignment. Unfortunately, it is difficult to assess the behavior of Q_t directly where the alignment occurs because of the inability to extract lifetimes from the 1175-keV doublet that occurs there (see Sec. III B1). At spins above the band crossing [$I > (\frac{29}{2})$], the average Q_t value (2.6 eb excluding lower-limit values) is somewhat smaller than that below the crossing [3.1 eb for $I < (\frac{23}{2})$], in fair qualitative agreement with the expectations of both CWS and PSM calculations. As mentioned earlier, this reduction in Q_t has been associated [9] with a structure change that occurs as a result of a proton alignment. The results of this work seem to verify this interpretation, although the Q_t values above the alignment should be interpreted with caution, since they are the ones that have the largest uncertainties associated with them in this band. Nevertheless, the sharp alignment observed in this band can only be understood if there is either some triaxiality present and/or the quadrupole deformation is very small [9], but the measured Q_t values unambiguously exclude the latter possibility. Even a slight reduction in collectivity is consistent with the onset of triaxiality (which evolves from a prolate shape at low spin) near and above the band-crossing region, according to CWS calculations [8,9].

A similar qualitative behavior of experimental Q_t values as a function of spin was observed recently in even-even ^{74}Kr [33]. Large, nearly constant values of Q_t ($\approx$2.9 eb) at low spin in the ground-state band showed a somewhat gradual decrease through the band-crossing region, followed by a set of constant, but smaller, Q_t values (2.1 eb) above the band crossing. These results were interpreted [33] as a consequence of the simultaneous alignment of $g_{9/2}$ protons and neutrons and were supported by CWS calculations, which also predicted a dramatic shape change beyond the alignment. Therefore, it may likely be the case that four particles are not contributing to the collective behavior after the band crossing in ^{74}Kr, and thus the shape change after the band crossing is more pronounced (as emphasized in Ref. [33]) than it is in ^{79}Sr.

A comparison of the experimental Q_t values in the $[422]\frac{5}{2}^+$ bands of ^{79}Sr and its neighboring isotope ^{81}Sr [4–6] and isotone ^{77}Kr [34,35] are shown in the top panel of Fig. 10. In general, the Q_t values in ^{79}Sr are systematically larger than those in ^{81}Sr and ^{77}Kr, indicating larger deformation. This is probably due to the combined influence of the proton number of Sr, which is nearer to midshell than that of Kr, and the importance of the position of the $N = 41$ Fermi level compared to the $N = 43$ one. Like ^{79}Sr, there is a rather sharp drop in the Q_t values of ^{77}Kr near the region of a $g_{9/2}$ proton alignment [34], and the average Q_t value is somewhat smaller above it. The observed pattern is nearly opposite for ^{81}Sr, where the average Q_t value is somewhat larger above the band-crossing region rather than below.

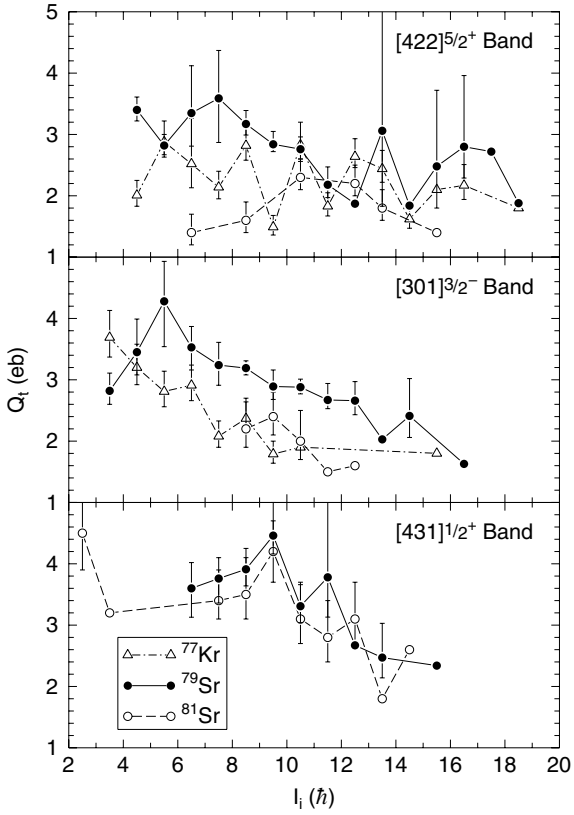

FIG. 10. Transition quadrupole moments Q_t as a function of the initial-state spin I_i for the $[422]\frac{5}{2}^+$ (top), $[301]\frac{3}{2}^-$ (middle), and $[431]\frac{1}{2}^+$ (bottom) bands in ^{77}Kr [34,35], ^{79}Sr, and ^{81}Sr [4–6]. Symbols without error bars indicate lower limits established from effective lifetime measurements.

The changes in the ^{81}Sr Q_t values become most pronounced near the onset of a 3-qp band crossing that occurs near spin $\frac{21}{2}$ and is accompanied by a significant decrease in the amount of signature splitting [5]. The associated $B(M1)$ strengths, inferred from previous lifetime measurements [5], increase with spin above the band-crossing region. (The pattern of $B(M1)$ strengths cannot be established below the alignment, mostly because only two $M1/E2$ transitions were observed there [5,7].) In contrast, the $B(M1)$ values in the $[422]\frac{5}{2}^+$ band of ^{77}Kr show large alternations that increase with spin, where the values are larger (smaller) for transitions having initial spin in the favored $\alpha = +\frac{1}{2}$ (unfavored $\alpha = -\frac{1}{2}$) signature. In this regard, the behavior of the $B(M1)$ values of this band in ^{79}Sr is much more similar to that of ^{77}Kr than of ^{81}Sr, as shown in the top panel of Fig. 11. This similarity is expected from a theoretical standpoint since the alternations in $B(M1)$ strengths are related to the signature splitting [36–39], and the degree and behavior of the signature splitting with spin in this band in ^{79}Sr is much closer to that of ^{77}Kr than that of ^{81}Sr. Alternating $B(M1)$ strengths are also predicted by the PSM, which shows excellent agreement between the predicted and experimental values in ^{79}Sr for this band (see Fig. 11).

It is interesting to note the considerable variation in the signature splitting observed in the 1-qp $[422]\frac{5}{2}^+$ intrinsic

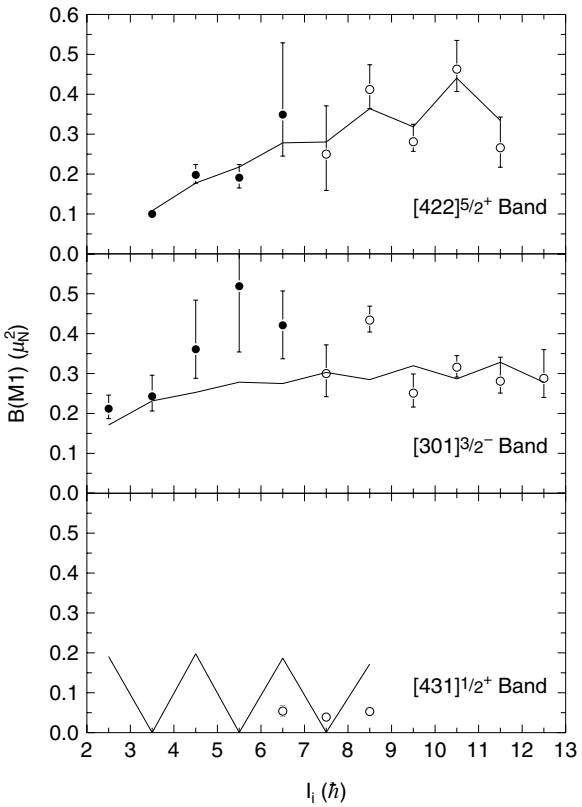

FIG. 11. Magnetic dipole transition strengths $B(M1)$ as a function of the initial-state spin I_i for the $[422]\frac{5}{2}^+$ (top), $[301]\frac{3}{2}^-$ (middle), and $[431]\frac{1}{2}^+$ (bottom) bands in ^{79}Sr. Filled (open) symbols represent experimental values deduced from measured [1,8] (estimated) quadrupole-dipole mixing ratios δ. (See text for an explanation of how the values of δ were estimated for a particular band.) The solid lines represent theoretical predictions from projected shell-model calculations.

structures of the light Sr isotopes as $N = Z$ is approached. For example, at $\hbar\omega = 0.35$ MeV it is almost zero in ^{77}Sr [1,40], about 120 keV in ^{79}Sr, and about 300 keV in ^{81}Sr [5,7]. This indicates a strong variation in deformation and shape with quasineutron occupation of the $g_{9/2}$ subshell. (If, however, all three of these Sr isotopes had similar prolate shapes, the changes in signature splitting would be exactly opposite to the observed behavior [5].) It is therefore reasonable to expect that ^{79}Sr, lying between ^{77}Sr and ^{81}Sr, can possess shape characteristics in this band that fall somewhere between the strongly deformed, prolate shape of ^{77}Sr [1] and the more weakly deformed, near-oblate shape of ^{81}Sr [5].

D. $[301]\frac{3}{2}^-$ band

The Q_t values associated with transitions in the yrast negative-parity band, suggested [1,8,9,12] to be based on the $[301]\frac{3}{2}^-$ Nilsson orbital, are shown in the middle panel of Fig. 9. A smooth decrease with increasing spin is indicated, beginning above the spin $\frac{17}{2}$ state. This behavior is consistent with the picture of a very gradual proton alignment that takes place over a broad range of spins, an interpretation suggested from the behavior of the kinematic moments of inertia $J^{(1)}$ determined experimentally [8,9,12] and calculated using the PSM [12], which show a smooth rise with angular frequency (until a much sharper alignment occurs at $\hbar\omega \approx 0.8$ MeV). However, the conventional wisdom that larger moments of inertia correspond to higher collectivity does not apply in this case. Part of the reason may be due to the more complicated wave functions resulting from strong f-p orbital mixing in the negative-parity structures due to the Coriolis interaction. Still, this particular concurrent behavior of $J^{(1)}$ and Q_t with spin is not unique to the $[301]\frac{3}{2}^-$ band of ^{79}Sr. It has also been observed in other yrast negative-parity bands in this mass region that are also suspected to be based on this same configuration, including the quasineutron (quasiproton) excitation in ^{77}Kr [34] (^{81}Y [17]). A rotationally induced depopulation of certain quasiparticle orbitals has been suggested [41] as a possible cause of a simultaneous increase in the moment of inertia while the quadrupole moment decreases. Figure 9 also shows the predictions of the CWS and PSM calculations. Both models fail to predict a significant decrease in Q_t with spin. In fact, the CWS predictions show little if any reduction in Q_t at all. The average magnitude of the Q_t values is better represented by the PSM calculations than the CWS calculations.

A comparison of the experimental Q_t values in similar bands based on the $[301]\frac{3}{2}^-$ configuration in ^{77}Kr [34,35], ^{79}Sr, and ^{81}Sr [5] is shown in the middle panel of Fig. 10. Both ^{77}Kr and ^{79}Sr show a similar pattern with spin, although perhaps the ^{77}Kr values decrease more rapidly with spin. (It should be noted that these values reflect a high-spin rearrangement of the level scheme that was performed in Ref. [35], and thus the pattern looks slightly different than the one presented in Fig. 10 of Ref. [34].) It is difficult to establish the pattern in ^{81}Sr due to the lack of sufficient mean lifetime information at low spin. Nevertheless, the magnitude of the values at higher spin seem to be closer to the ^{77}Kr values than the ^{79}Sr ones. In fact, the ^{79}Sr values are systematically larger than those in both ^{77}Kr and ^{81}Sr, indicating that ^{79}Sr is more deformed in this configuration over a broad range of spins.

The $B(M1)$ values representative of the $\Delta I = 1$ transitions in the $[301]\frac{3}{2}^-$ band of ^{79}Sr are shown along with the predictions of the PSM in the middle panel of Fig. 11. Like the $[422]\frac{5}{2}^+$ band, the values increase with spin near the band head, then form an alternating pattern at higher spin. However, the magnitude of the alternations are much smaller than that observed for the $[422]\frac{5}{2}^+$ band and appear to oscillate about a (roughly) constant value, unlike the case in the $[422]\frac{5}{2}^+$ band. A remaining puzzle concerns the disagreement in the phase of the alternations between the experimental values and those predicted by the PSM (see Fig. 11). However, one should view this disagreement with caution since the rather small magnitude of the alternations, coupled with the error bars associated with the experimental values, also allows for an alternating pattern with the opposite phase above spin $\frac{19}{2}$. The experimental $B(M1)$ values above spin $\frac{13}{2}$ were also estimated using an average quadrupole-dipole mixing ratio $\delta = -0.14(6)$ representative of the available measured values

in this band, although the exact value used will not affect the $B(M1)$ values much unless it was very different from this assumed value. It should also be noted that the behavior of the experimental $B(M1)$ values in the $[301]\frac{3}{2}^-$ band of ^{77}Kr [34] shows an alternating pattern with a phase that agrees with that observed in ^{79}Sr, although there is an overall decrease, rather than increase, in $M1$ strength with spin. Too few $\Delta I = 1$ transitions were observed in the $[301]\frac{3}{2}^-$ band of ^{81}Sr to draw meaningful comparisons with ^{79}Sr.

E. $[431]\frac{1}{2}^+$ band

The Q_t values associated with $E2$ transitions in the $[431]\frac{1}{2}^+$ band of ^{79}Sr are shown in the bottom panel of Fig. 9 along with the predictions of CWS and PSM calculations. The average experimental value of about 3.6 eb suggests an average quadrupole deformation $\beta_2 \approx 0.41$ and confirms an earlier prediction based on CWS calculations [6] that the $[431]\frac{1}{2}^+$ band in ^{79}Sr carries larger collectivity and deformation than a similar band in ^{81}Sr, a result that can be interpreted graphically from the bottom panel of Fig. 10. The calculations in fact predict that the deformation associated with this configuration should peak in the odd Sr isotopes at $N = 41$ (^{79}Sr), although states belonging to this intrinsic configuration have yet to be identified experimentally in ^{77}Sr. The PSM calculations also predict large Q_t values for this band in ^{79}Sr, although in this case the CWS calculations in general agree somewhat better with the experimental values than the PSM calculations. Nevertheless, the PSM predicts correctly the band based on this configuration to be the most highly deformed of the three observed bands in ^{79}Sr (see Fig. 9), in agreement with the predictions of the CWS calculations and the experimental results. Below spin $(\frac{23}{2})$, the experimental values remain roughly constant, a behavior that is supported qualitatively by both calculations, although there are noticeable irregularities to this pattern that occur at spins $(\frac{19}{2})$ and $(\frac{27}{2})$ (see Fig. 9). The jump in Q_t at spin $(\frac{19}{2})$ cannot be explained by either the CWS or PSM calculations, and it is difficult to deduce a physical reason for this change since there is no other evidence for a structure change there [12]. Still, it is interesting that a similar jump in Q_t occurs at the same spin state in the $[431]\frac{1}{2}^+$ band of ^{81}Sr (see Fig. 10). The drop in the ^{79}Sr Q_t value at spin $(\frac{27}{2})$ could be related to the suggested gradual proton alignment that occurs in this band, as supported by PSM calculations which indicate a gradual increase in $J^{(1)}$ with spin [12] accompanied by a slow decrease in Q_t (see Fig. 9). However, the observed drop in Q_t is much larger than that predicted by the PSM in this spin range. More lifetime measurements at higher spin would be necessary to help understand this discrepancy.

Lifetime information in other bands based on the $[431]\frac{1}{2}^+$ configuration in this mass region remain sparse, but there could be at least one additional indication of the deformation-driving nature of the intruder $d_{5/2}$ orbital that it belongs to from a recent study of ^{77}Kr [35]. Although a 1-qp band based on the $[431]\frac{1}{2}^+$ configuration has not been identified in this nucleus, a 3-qp band was found which was suggested to be based on the $\nu[431]\frac{1}{2}^+ \otimes \pi[312]\frac{3}{2}^- \otimes \pi[431]\frac{3}{2}^+$ configuration leading to a highly deformed, near-prolate shape with $\beta_2 \approx 0.35$ based on CWS calculations. This prediction is at least partially supported by a lifetime measurement of one state in this band, which was originally thought to belong to the $[301]\frac{3}{2}^-$ band [34]. The Q_t value associated with the $E2$ decay of this state implies $\beta_2 \approx 0.37$, much higher than for the states in the $[301]\frac{3}{2}^-$ band but which is consistent with the expectations of a band with quasiparticle occupation of the $d_{5/2}$ orbital.

However, very recently an alternative interpretation of this 3-qp band was proposed which does not involve occupation of the $d_{5/2}$ orbital [42]. This description, supported by configuration-dependent cranked Nilsson-Strutinsky calculations [43,44], involves a configuration with three protons and five neutrons in the $g_{9/2}$ shell only. Regardless of the interpretation of this band, however, its inherent configuration is clearly much different from that of the $[431]\frac{1}{2}^+$ band in ^{79}Sr, thus making it a difficult case for comparison. It should also be mentioned that a rotational band which shows many similarities to the $[431]\frac{1}{2}^+$ band in ^{79}Sr was identified recently in the $N = 41$ isotone ^{81}Zr [12], but lifetime measurements are unavailable in this band (or in any of the other observed bands in this nucleus for that matter) to provide another systematic comparison.

The $B(M1)$ strengths for this band in ^{79}Sr are weak in comparison to those in the $[422]\frac{5}{2}^+$ and $[301]\frac{3}{2}^-$ bands and perhaps show a slight alternating pattern with spin, as shown in the bottom panel of Fig. 11. The PSM calculations also predict an alternating pattern with a phase that agrees with the experimental results, although the magnitude of the alternations are nearly ten times as large as the experimental ones. Nevertheless, the PSM calculations predict correctly the qualitative differences in the $B(M1)$ values for the three bands. While the data are sparse for the $[431]\frac{1}{2}^+$ band, the PSM calculations account for the significant decrease in magnitude of the $B(M1)$ values reasonably well.

V. SUMMARY

High-spin states in ^{79}Sr were studied using the ^{54}Fe(^{28}Si, $2pn$) reaction at 90 MeV performed at the FSU Tandem-Superconducting LINAC accelerator. The isotopically enriched ^{54}Fe target was thick enough to stop all recoils and hence allowed for the measurement of lifetimes using the DSAM. γ rays were detected in prompt coincidence using the FSU Compton-suppressed Ge array consisting of three high-efficiency Clover detectors and seven single-crystal detectors. The γ-γ coincidences were used to confirm the existing level scheme of ^{79}Sr in three separate rotational band structures using coincidence relations, intensity and effective lifetime measurements, and DCO ratios. The lifetimes of 33 excited states were measured using the DSAM, with the experimental line shapes obtained at two separate detector angles and by gating from above the transitions of interest whenever possible. Some side-feeding lifetimes were measured by comparing the analyses of line-shape spectra obtained by gating from above and below a de-exciting transition from the state of interest.

Transition quadrupole moments Q_t inferred from the lifetimes measured in the yrast positive-parity band (suggested to be based on the $[422]\frac{5}{2}^+$ Nilsson configuration) suggest a strongly deformed structure with an average quadrupole deformation $\beta_2 \approx 0.34$ assuming axial symmetry. The Q_t values drop rather suddenly near the region of a proton alignment, then rise again above the alignment to an average value somewhat smaller than below the alignment. The general trend of a decreasing Q_t with spin is supported by the PSM and CWS calculations, but in general there is not quantitative agreement between the experimental values and the predictions of both models. The $B(M1)$ values in this band show an alternating pattern that develops with increasing spin, in excellent agreement with the PSM calculations.

The experimental Q_t values in the yrast negative-parity band (suggested to be based on the $[301]\frac{3}{2}^-$ Nilsson configuration) are large (between about 2.4 and 4.3 eb) over a wide range of spins but show a gradual decrease with spin that is attributed to the gradual proton alignment that is suggested to take place in the same spin range. A very similar behavior has been observed in the $[301]\frac{3}{2}^-$ band of ^{77}Kr. The $B(M1)$ values in this band first increase with spin near the bandhead, then develop a small alternating pattern at high spin. The alternating pattern is opposite in phase compared to the predictions of the PSM, although experimental uncertainty could account for the difference.

The lifetimes measured in a band suggested to be based on the $[431]\frac{1}{2}^+$ intrinsic Nilsson configuration represent only the second such measurement of a 1-qp band with this configuration in the mass 80 region. As was the case in ^{81}Sr, the inferred values of Q_t in this band in ^{79}Sr suggest very strong deformation ($\beta_2 \approx 0.41$ assuming axial symmetry) for this structure, even larger than that determined experimentally for ^{81}Sr. This further demonstrates the strong deformation-driving characteristics of the $d_{5/2}$ intruder orbital in this mass region, as predicted by both the CWS and PSM models. The $B(M1)$ values in this band show little if any evidence for an alternating pattern based on the three available data points, but the PSM calculations indicate a strong alternating pattern with spin.

ACKNOWLEDGMENTS

This work was supported in part by the U. S. National Science Foundation through grants PHY-99-70991 (FSU), PHY-0140324, and PHY-0216783 (Y.S.), as well as the Ohio Wesleyan University Summer Science Research Program. We thank W. Nazarewicz for providing the results of his cranked Woods-Saxon calculations, and the staff of the FSU Tandem-Superconducting LINAC facility for their support throughout the experiment.

[1] C. J. Lister, B. J. Varley, H. G. Price, and J. W. Olness, Phys. Rev. Lett. **49**, 308 (1982).
[2] R. F. Casten, Phys. Rev. Lett. **54**, 1991 (1985).
[3] W. Nazarewicz, J. Dudek, R. Bengtsson, T. Bengtsson, and I. Ragnarsson, Nucl. Phys. **A435**, 397 (1985).
[4] S. E. Arnell, C. Ekström, L. P. Ekström, A. Nilsson, I. Ragnarsson, P. J. Smith, and E. Wallander, J. Phys. G **9**, 1217 (1983).
[5] E. F. Moore, P. D. Cottle, C. J. Gross, D. M. Headly, U. J. Hüttmeier, S. L. Tabor, and W. Nazarewicz, Phys. Rev. C **38**, 696 (1988).
[6] E. F. Moore, P. D. Cottle, C. J. Gross, D. M. Headly, U. J. Hüttmeier, S. L. Tabor, and W. Nazarewicz, Phys. Lett. **B211**, 14 (1988).
[7] D. H. Smalley, R. Chapman, P. J. Dagnall, C. Finck, B. Haas, M. J. Leddy, J. C. Lisle, D. Prévost, H. Savajols, and A. G. Smith, Nucl. Phys. **A611**, 96 (1996).
[8] J. Heese, K. P. Lieb, S. Ulbig, B. Wörmann, J. Billowes, A. A. Chishti, W. Gelletly, C. J. Lister, and B. J. Varley, Phys. Rev. C **41**, 603 (1990).
[9] A. A. Chishti, W. Gelletly, C. J. Lister, B. J. Varley, and Ö. Skeppstedt, J. Phys. G: Nucl. Part. Phys. **16**, 481 (1990).
[10] M. A. Cardona, G. García Bermúdez, A. Filevich, and E. Achterberg, Phys. Rev. C **41**, 2403 (1990).
[11] S. Suematsu, S. Mitarai, J. Mukai, H. Tomura, A. Odahara, T. Kuroyanagi, S. E. Arnell, Ö. Skeppstedt, D. Jerrestam, J. Nyberg, A. Atac, H. Roth, and G. Sletten, Kyushu Univ. Tandem Acc. Lab. Report, 1991–1992, p. 72 (1993).
[12] N. Mărginean, D. Bucurescu, C. Rossi Alvarez, C. A. Ur, Y. Sun, D. Bazzacco, S. Lunardi, G. de Angelis, M. Axiotis, E. Farnea, A. Gadea, M. Ionescu-Bujor, A. Iordăchescu, W. Krolas, Th. Kröll, S. M. Lenzi, T. Martinez, R. Menegazzo, D. R. Napoli, P. Pavan, Zs. Podolyak, M. De Poli, B. Quintana, and P. Spolaore, Phys. Rev. C **69**, 054301 (2004).
[13] K. Hara and Y. Sun, Int. J. Mod. Phys. E **4**, 637 (1995).
[14] http://fsunuc.physics.fsu.edu/~caussyn/
[15] J. F. Ziegler, J. P. Biersack, and U. Littmark, *The Stopping and Range of Ions in Matter* (Pergamon, New York, 1985).
[16] http://www.SRIM.org
[17] R. A. Kaye, C. T. Rastovski, S. L. Tabor, J. Döring, F. Cristancho, M. Devlin, G. D. Johns, I. Y. Lee, F. Lerma, A. O. Macchiavelli, D. G. Sarantites, and G. Z. Solomon, Phys. Rev. C **66**, 054305 (2002).
[18] M. Wiedeking, S. L. Tabor, F. Cristancho, M. Devlin, J. Döring, C. B. Jackson, G. D. Johns, R. A. Kaye, I. Y. Lee, F. Lerma, A. O. Macchiavelli, M. Naidu, I. Ragnarsson, D. G. Sarantites, and G. Z. Solomon, Phys. Rev. C **67**, 034320 (2003).
[19] R. A. Kaye, O. Grubor-Urosevic, S. L. Tabor, J. Döring, Y. Sun, R. Palit, J. A. Sheikh, T. Baldwin, D. B. Campbell, C. Chandler, M. W. Cooper, S. M. Gerbick, C. R. Hoffman, J. Pavan, L. A. Riley, and M. Wiedeking, Phys. Rev. C **69**, 064314 (2004).
[20] F. Cristancho and K. P. Lieb, Nucl. Phys. **A486**, 353 (1988).
[21] S. L. Tabor, J. Döring, J. W. Holcomb, G. D. Johns, T. D. Johnson, T. J. Petters, M. A. Riley, and P. C. Womble, Phys. Rev. C **49**, 730 (1994).
[22] F. Cristancho, K. P. Lieb, J. Heese, C. J. Gross, W. Fieber, Th. Osipowicz, S. Ulbig, K. Bharuth-Ram, S. Skoda, J. Eberth, A. Dewald, and P. von Brentano, Nucl. Phys. **A501**, 118 (1989).
[23] M. Wiedeking, R. A. Kaye, G. Z. Solomon, S. L. Tabor, J. Döring, G. D. Johns, F. Cristancho, M. Devlin, F. Lerma,

D. G. Sarantites, I. Y. Lee, and A. O. Macchiavelli, Phys. Rev. C **62**, 024316 (2000).
[24] R. Palit, J. A. Sheikh, Y. Sun, and H. C. Jain, Nucl. Phys. **A686**, 141 (2001).
[25] R. Palit, J. A. Sheikh, Y. Sun, and H. C. Jain, Phys. Rev. C **67**, 014321 (2003).
[26] Y. Sun, Eur. Phys. J. A **20**, 133 (2004).
[27] Y. Sun and J. L. Egido, Nucl. Phys. **A580**, 1 (1994).
[28] R. Wyss, F. Lidén, J. Nyberg, A. Johnson, D. J. G. Love, A. H. Nelson, D. W. Banes, J. Simpson, A. Kirwan, and R. Bengtsson, Nucl. Phys. **A503**, 244 (1989).
[29] W. Nazarewicz, M. A. Riley, and J. D. Garrett, Nucl. Phys. **A512**, 61 (1990).
[30] J. Dudek, W. Nazarewicz, and P. Olanders, Nucl. Phys. **A420**, 285 (1984).
[31] I. Hamamoto and B. R. Mottelson, Phys. Lett. **B132**, 7 (1983).
[32] P. Ring, A. Hayashi, K. Hara, H. Emling, and E. Grosse, Phys. Lett. **B110**, 423 (1982).
[33] A. Algora, G. de Angelis, F. Brandolini, R. Wyss, A. Gadea, E. Farnea, W. Gelletly, S. Lunardi, D. Bazzacco, C. Fahlander, A. Aprahamian, F. Becker, P. G. Bizzeti, A. Bizzeti-Sona, D. de Acuña, M. De Poli, J. Eberth, D. Foltescu, S. M. Lenzi, T. Martinez, D. R. Napoli, P. Pavan, C. M. Petrache, C. Rossi Alvarez, D. Rudolph, B. Rubio, S. Skoda, P. Spolaore, R. Menegazzo, H. G. Thomas, and C. A. Ur, Phys. Rev. C **61**, 031303(R) (2000).
[34] T. D. Johnson, J. W. Holcomb, P. C. Womble, P. D. Cottle, S. L. Tabor, F. E. Durham, S. G. Buccino, and M. Matsuzaki, Phys. Rev. C **42**, 2418 (1990).
[35] G. N. Sylvan, J. Döring, G. D. Johns, S. L. Tabor, C. J. Gross, C. Baktash, H.-Q. Jin, D. W. Stracener, P. F. Hua, M. Korolija, D. R. LaFosse, D. G. Sarantites, F. Cristancho, E. Landulfo, J. X. Saladin, B. Cederwall, I. Y. Lee, A. O. Macchiavelli, W. Rathbun, and A. Vander Molen, Phys. Rev. C **56**, 772 (1997).
[36] I. Hamamoto and H. Sagawa, Nucl. Phys. **A327**, 99 (1979).
[37] I. Hamamoto, Phys. Lett. **B106**, 281 (1981).
[38] F. Dönau, Nucl. Phys. **A471**, 469 (1987).
[39] M. Matsuzaki, Phys. Rev. C **39**, 691 (1989).
[40] C. J. Gross, C. Baktash, D. M. Cullen, R. A. Cunningham, J. D. Garrett, W. Gelletly, F. Hannachi, A. Harder, M. K. Kabadiyski, K. P. Lieb, C. J. Lister, W. Nazarewicz, H. A. Roth, D. Rudolph, D. G. Sarantites, J. A. Sheikh, J. Simpson, Ö. Skeppstedt, B. J. Varley, and D. D. Warner, Phys. Rev. C **49**, R580 (1994).
[41] J. D. Garrett, J. Nyberg, C. H. Yu, J. M. Espino, and M. J. Godfrey, in *International Conference on Contemporary Topics in Nuclear Structure Physics*, edited by R. Casten, A. Frank, M. Moshinsky, and S. Pittel (World Scientific, Singapore, 1988), p. 699.
[42] T. Steinhardt, J. Eberth, and I. Ragnarsson (unpublished).
[43] T. Bengtsson and I. Ragnarsson, Nucl. Phys. **A436**, 14 (1985).
[44] A. V. Afanasjev, D. B. Fossan, G. J. Lane, and I. Ragnarsson, Phys. Rep. **322**, 1 (1999).